
**UNIVERSITY OF THE PHILIPPINES**

**Bachelor of Science in Physics**

**Lemuel Gavin G. Saret**

# *Photon scattering by an Alcubierre warp drive space-time*

Thesis Adviser:
**Michael Francis Ian Vega II, Ph.D.**
**National Institute of Physics**
**University of the Philippines Diliman**

Date of Submission:
June 2020

Thesis Classification:
**P**

*This thesis is available to the public*

"What is the single most important thing that you want your readers to learn? My answer: the amazing power of the human mind – by fits and starts, blind alleys, and leaps of insight – to unravel the complexities of our Universe, and reveal the ultimate simplicity, the elegance, and the glorious beauty of the fundamental laws that govern it."

*– Kip S. Thorne, Black Holes & Time Warps: Einstein's Outrageous Legacy*

# Acknowledgments

I would like to express my sincerest gratitude to those who supported me in finishing this thesis and to those who have been part of my journey as a college student.

First and foremost, to the Almighty and everliving God, the foundation of my life. You have been my constant source of joy and strength. I praise and thank you for granting me the knowledge and wisdom that I need to finish my thesis and degree.

To the Department of Science and Technology, thank you for financially supporting my college education. May you continue to support the Filipino youth in pursuing careers in the different branches of science.

To **Sir Ian Vega**, our beloved mentor, I aspire to be an educator and researcher like you. It is your passion for knowledge that first motivated me to apply in the Theoretical Physics Group - Gravity Group. I truly enjoyed working under your supervision as I learned a lot about life in general from our frequent interactions. Thank your for being patient with me and imparting some of your knowledge and skills with me – even though I process some information really slowly at times – as I was able to use a lot of them in this thesis.

To the Gravity-Theory Group, thank you for creating an environment that fosters to the curious minds of aspiring scientists. Special mentions to **Jane**, **Adrian V.**, **Regi**, **Sean**, **Jerome**, **John**, **Adrian B.**, and **Marc**, my seniors in the lab. I appreciate all the night outs, along with the intellectual and the not so intellectual conversations that we had. Thank you for answering all my basic inquiries, supporting me when I'm facing difficulties, and for overall making my lab life special.

To Christ's Youth in Action QC Hub, my refuge for my 5 year stay in college, I have seen the face of Christ in your service to God and one another. I want to specially thank the staffers and the student leaders of this organization for being excellent witnesses of God's love to us. Keep on keeping on, brothers and sisters! Kay Kristo Buong Buhay Habambuhay!

To the UP Physics Association, I will always cherish the friendships and memories that I built while being part of this organization. Thank you for giving me the opportunity to lead and serve the NIP and UP community through our initiatives.

To Stillwolves/Stillwolves NG, my ultimate family, I thank all of you for welcoming me wholeheartedly in the team. Special mentions to **Kuya Jun**, **Kuya Perry**, **Kuya Edsent**, **Kuya Jays**, **Ate France**, **Nemu**, **Arny**, **Jazh**, **Marvinn**, **Lo**, **Iggy**, **Is**, **Lexi**, **Danye**, **Yssa**. Thank you for all the pun times before, during, and after trainings and tournaments. I hope to see you on the field soon!

To ma$\hbar$ bois composed of **Matt**, **Marco**, **Buki**, **Kim**, and **Lance**, thank you for this brotherhood that continues to grow stronger. I will always cherish our wholesome memories together, along with our more wild and crazy adventures. I am confident that these friendships will transcend this lifetime. And please always remember, gusto ko happy ka!

To the regular goers of my MG composed of **Kuya Glen**, **Arvs**, **Jorik**, **Jopoy**, and **Diego**, thank you for being a physical, spiritual, and musical blessing to me. I appreciate all the lunch and coffee dates, and the random banters between us brothers.

To the Ifuguys, my housemates and brothers in Christ, I learned more about service and our faith our one and a half semester stay in the house hold. Thank you for inspiring me to become a better Christian.

To the Clowns and regular SB petron katip goers composed of **Cy**, **Jacob**, **Leo**, **Pat**, **Mark**, **Mawis**, **Ymman**, **Ares**, and **Liana**, I am eternally grateful for this group since I finished most of my thesis progress and requirements in our nightly thesis assemblies. Thank you for the support and the destress that you gave me through our board game, karaoke, and chika sessions. I would also like to send my congratulations for #sablay2020 in advance. I wish that we may all fulfill our hopes and dreams.

To my professors who left a lasting impression in my life, you all have perfectly emulated the "Utak at Puso" catchphrase of UP. I thank you for molding me to become the Isko I am today. I have seen your passion for your respective fields and I am genuinely inspired to keep on striving to become a better person because of all the lessons I learned both inside and outside the classroom. Padayon!

Finally to my parents, **Benny** and **Meg**, and to my brother, **Amiel**, I dedicate all my achievements to you. Thank you for never failing to support me in my endeavors in your own respective ways. I may have been physically away the past 5 years, but know that I love and care for all of you. I hope that I made you all proud.

## ABSTRACT

### PHOTON SCATTERING BY AN ALCUBIERRE WARP DRIVE SPACE-TIME

**Lemuel Gavin G. Saret**
**University of the Philippines (2020)**

**Adviser:**
**Michael Francis Ian Vega II, Ph.D.**

We study the scattering of incoming photons by an incoming or outgoing "warp bubble". Specifically, we numerically integrate the null geodesic equations in the Alcubierre warp drive space-time and characterize the resulting changes in the photons. We find that for an observer in a distant reference frame, light rays interacting with the warp drive are deflected and experience net blue-shifts whose magnitudes depend non-trivially on the photon's impact parameter, the warp drive velocity, and the warp bubble width. We find that there is a corresponding increase in angular deflections and overall blue-shift for higher values of the warp velocity, and a corresponding decrease for higher values of the warp bubble width. Meanwhile, images that propagate through the warp drive distortion would experience gravitational lensing that would invert a radial area of the image from the center outward as seen by an observer behind the said warp drive. This lensing effect is caused by the negative energy density matter that supports the warp drive space-time.

PACS: 04.40.-b (Self-gravitating systems; continuous media and classical fields in curved spacetime), 04.25.-g ( Approximation methods; equations of motion)

# Table of Contents

# List of Figures

# Chapter 1

# Introduction

## 1.1 Background of the study

Faster-than-light (FTL) travel is one of the most interesting notions in science fiction. This allows a space explorer to travel light year distances in a matter of seconds or minutes by travelling with speeds faster than the speed of light. FTL travel is practically essential for stories involving space travel and exploration because of the vastness of the real universe. Let us consider travel from the Earth to Proxima Centauri as an example, it will take the Parker Solar Probe, considered the fastest man-made object with a maximum speed of $692,000$ km/hr, $7$ thousand years to fly to Proxima Centauri. Even if we travelled at the speed of light, it would still take us about $4$ years to reach the nearest star to Earth. Similarly, If we want to travel far, far away, we'll need to find a way of getting there within our life time because I'm pretty sure that everyone would agree that Star Wars and Star Trek would be incredibly boring if travel took years rather than minutes or hours.

Interestingly, different scientific fiction realms like Star Wars and Star Trek discuss different methods to achieve apparent FTL travel. In Star Wars, a spacecraft can enter a different dimension called "hyperspace" wherein certain laws of physics like the speed of light and relativity don't apply. Travelling through the hyperspace allows a spaceship to travel distances at speeds greater than the speed of light, and return to the the normal space once it reaches its destination. On the other hand, Star Trek introduces the concept of a static warp bubble or field that creates a subspace bubble with the help of warp fields that distort the space-time continuum, thus allowing FTL travel.

However, since Albert Einstein's proposal of the Special Theory of Relativity in

1905, physics students and practitioners have always operated under the restriction that nothing can move faster than the speed of light. Hence, there will be no such thing as faster-than-light travel or exploration. Meanwhile, in general relativity (GR) we consider a more precise version of this rule: in general relativity, we learn that nothing can locally travel faster than the speed of light. In fact, previous solutions to the Einstein field equations show that it is theoretically possible to provide unique spacetimes that allow FTL travel without violating the laws of special relativity [1–10]

To provide his own solution to this restriction, Miguel Alcubierre [11] came up with a space-time which has features similar to the "warp drive" which is more commonly known as the "hyper drive" usually found in science fiction lore. The Alcubierre solution allows a "spaceship" to have an apparent speed which is much greater than the speed of light relative to a distant observer. This phenomena can be described as a distortion of the fabric of space-time in a wave-like manner. This phenomena causes the space ahead of the spaceship to contract while the space behind of the spaceship to expand. In this way, the spaceship will be pushed away from its source and pulled towards a destination by the space-time curvature. In this space-time, passengers on the spaceship can travel arbitrary large distances over small amounts of proper time; further there is no time dilation effects experienced between the spaceship and clocks outside the region affected by the warp drive.

However, as Ken Olum demonstrated, the idea of superluminal travel is intimately related to negative energy densities [12]. Similarly, the Alcubierre warp drive space-time has properties that make it physically impossible. In order to create such distortion in space-time, "exotic" matter is required, one which violates the weak, strong, and dominant energy conditions [13–17]. Although quantized fields can locally violate the energy conditions, an analysis by Pfenning and Ford [18] discussed that the total integrated energy density required to maintain the warp drive curvature is physically unattainable. Specifically, for warp drive space-times, by using the quantum inequality discussed by Ford and Roman [19], along with their other supplementary work [20], it was verified that unphysical amounts of energy are required to sustain the warp drive. On the other hand, Van Den Broeck has recently shown how to significantly reduce the amount of negative energy density matter required for the warp drive to the order of grams [21]. Similarly, a study by

Lobo [22] suggested that even at low warp speeds, the net negative energy required to sustain the warp drive curvature must be a significant factor of the mass of the space ship.

## 1.2 Problem Statement

Despite the difficulties and limitations in the construction of the Alcubierre warp drive, it is interesting to ask how light gets scattered as it moves through the the vicinity of the warp bubble as similarly done in other compact object systems. We consider photons originating from infinity and initially moving parallel to an incoming Alcubierre warp bubble. We wish to characterize what happens to the photons according to a faraway observer. We study the null geodesic equations for a photon as it traverses the vicinity of an Alcubierre warp drive. The resulting trajectory and momenta equations are then used to determine the angular deflections and energy shifts of protons as it collides with the moving warp bubble. We adjust values of the warp speed, warp bubble width, and impact parameter to determine the changes in deflection angle and energy shifts as the photons collide with a faster and thicker warp bubble.

## 1.3 Significance of the Study

Albert Einstein suggested that gravity is the warping of space and time and is considered the curvature of the curvature caused by massive bodies, which determines the path objects would travel. Warp drives or warp drive space-times are among the most unique but strangest solutions of Einstein's general relativity, and have long captured the interest of both the scientific community and the general public. We study how the warp drive curvature affects the motion of photons and how this curvature would scatter a beam of light after collision. Along with the photon scattering, we also study how the Alcubierre distortion shifts the energy of light that passes through. This work will contribute to our understanding of warp drives and its effects on its environment.

## 1.4 Outline of the manuscript

This manuscript is divided into 6 chapters. Chapter II is dedicated to the introduction of the reader to the Alcubierre warp drive. This includes discussions about travel in the Alcubierre warp drive, a better visualization of the distortion, and its physical limitations and some proposed solutions. Along with this, we also devote this chapter for some preliminary discussion about General Relativity that will be useful in the later discussions. Chapter III solves for the photon trajectories and shifts in momenta for photons in the Alcubierre warp drive and gives us a brief overview of our system. Additionally, in Chapter III we compare our results to the results of Anderson et al. [23], which has been done using the Hamiltonian based geodesics. Chapter IV shows us the nature of light as it traverses the Alcubierre warp drive. The ray tracing of light as well as the the relation of the angular deflections with the impact parameters will be discussed for different values of the warp speed and warp bubble width. Chapter V will be dedicated to discussing the energy shifts, including the overall blue-shift, of photons in the Alcubierre warp drive for different values of the warp speed and warp bubble width. Finally, Chapter VI states the conclusion and recommendation for future studies.

# Chapter 2

# The Alcubierre warp drive

## 2.1 Basics of General Relativity

According to Edmund Bertschinger [24] there are three essential concepts underlying general relativity. First is the concept of space-time. The fabric of space-time is a mathematical structure called a pseudo-Riemannian manifold that combines the three-dimensional structure of space with time. In short, the dimensions of space and time together comprise a curved four-dimensional non-Euclidean geometry. Consequently, relativists must first be familiar with the fundamental geometrical properties of curved space-time. Specifically, the laws of physics must remain valid regardless of the choice of coordinate system that is used to determine points in space-time. These fundamental geometrical properties of curved space-time would be later introduced in this chapter.

The second concept is the concept of reference frames. According to GR, there exists a local inertial reference frame at every point in space-time. This corresponds to locally flat geometry observed by freely falling observers. This concept makes the physics in GR locally comparable to the physics in special relativity (SR) and makes it an extension of GR in curved space-time.

Last, is the concept of curvature. In the words of John Wheeler, "Space-time grips mass, telling it how to move. Mass grips space-time, telling it how to curve. This means that mass, along with the momentum flux, as Bertschinger mentioned, curves space-time in a manner described by Einstein's field equations.

These three ideas are highlighted when comparing Albert Einstein's general theory of relativity to Isaac Newton's concept of gravity. In Newtonian gravity, gravity is a downward force that influences objects in Euclidean space respective

of time. Meanwhile, there is no concept of gravitational force in GR. Rather, in the absence of charges and external forces, less massive objects would follow the shortest possible paths called geodesics through a space-time distortion curved by a more massive object. Free falling observers define local inertial reference frames. Space and time are not independent in GR and SR but are combined into a four-dimensional manifold called space-time.

Working with a GR concept such as the Alcubierre warp-drive requires some background on differential geometry. In the duration of this manuscript we will be discussing essential physics and mathematics needed to describe the physics in a curved space-time using notes and discussions from [25–31].

### 2.1.1 General Notation

In the duration of our review, we will adopt units in which the speed of light $c = 1$. Greek indices such as $\mu$ and $\nu$, will take values of $\{0, 1, 2, 3\}$, representing the time and three-dimensional spatial components of our tensors. The Einstein summation convention is assumed: repeated upper and lower indices are to be summed over their ranges, for example,

$$\begin{aligned} A^{\mu}B_{\mu} =& A^0B_0 + A^0B_1 + A^0B_2 + A^0B_3 + \\ & A^1B_0 + A^1B_1 + A^1B_2 + A^1B_3 + \\ & A^2B_0 + A^2B_1 + A^2B_2 + A^2B_3 + \\ & A^3B_0 + A^3B_1 + A^3B_2 + A^3B_3 \end{aligned} \tag{2.1}$$

Lastly, the flat space-time Minkowski metric components are

$$\eta_{\mu\nu} = \begin{pmatrix} -1 & 0 & 0 & 0 \\ 0 & 1 & 0 & 0 \\ 0 & 0 & 1 & 0 \\ 0 & 0 & 0 & 1 \end{pmatrix} \tag{2.2}$$

### 2.1.2 Vectors, Dual vectors, and Tensors

Consider a curve $\gamma$ on a manifold, parameterized by an arbitrary variable, $\lambda$, that can be described in an arbitrary coordinate system by $x^{\alpha}(\lambda)$. The rate rate of change of a scalar function $f(x^{\alpha})$ along this curve in this coordinate system is:

$$\frac{df}{d\lambda} = \frac{\partial f}{\partial x^{\alpha}}\frac{dx^{\alpha}}{d\lambda} = f_{,a}u^{\alpha} \tag{2.3}$$

where $u^\alpha = dx^\alpha/d\lambda$ is a vector that is tangent to $\gamma$ everywhere, and $f_{,\alpha} = \partial f/\partial x^\alpha$ is a dual vector and is the gradient of the function $f$. Under an arbitrary coordinate transform from $x^\alpha$ to $x^{\alpha'}$, these factors transforms into

$$f_{,\alpha'} = \frac{\partial f}{\partial x^{\alpha'}} = \frac{\partial f}{\partial x^\alpha}\frac{\partial x^\alpha}{\partial x^{\alpha'}} = \frac{\partial x^\alpha}{\partial x^{\alpha'}} f_{,\alpha} \tag{2.4}$$

and

$$u^{\alpha'} = \frac{dx^{\alpha'}}{d\lambda} = \frac{\partial x^{\alpha'}}{\partial x^\alpha}\frac{\partial x^\alpha}{\partial \lambda} = \frac{\partial x^{\alpha'}}{\partial x^\alpha} u^\alpha \tag{2.5}$$

From these equations, we find that $df/d\lambda$ can be further simplified into:

$$f_{,\alpha'} u^{\alpha'} = \left(\frac{\partial x^\alpha}{\partial x^{\alpha'}} f_{,\alpha}\right)\left(\frac{\partial x^{\alpha'}}{\partial x^\alpha} u^\alpha\right) = f_{,\alpha} u^\alpha \tag{2.6}$$

With this simplification we were able to prove that $df/d\lambda$ stays invariant under a coordinate transformation.

Next, we consider Eqns (2.4 - 2.5). Eqn. (2.4) is an example of a coordinate transform of a *vector*. A vector $A^\alpha$ transforms as

$$A^{\alpha'} = \frac{\partial x^{\alpha'}}{\partial x^\alpha} A^\alpha \tag{2.7}$$

Meanwhile, Eqn. (2.5) is an example of a coordinate transform of a *dual vector*. A dual vector $B_\alpha$ transforms as

$$B_{\alpha'} = \frac{x^\alpha}{\partial x^{\alpha'}} B_\alpha \tag{2.8}$$

The contraction between any vector and dual vector, $A^\alpha B_\alpha$ for example, is scalar and invariant under a coordinate transform. In general, an object $T^{\alpha\ldots\beta}{}_{\gamma\ldots\delta}$ that transforms like

$$T^{\alpha'\ldots\beta'}{}_{\gamma'\ldots\delta'} = \frac{\partial x^{\alpha'}}{\partial x^\alpha}\ldots\frac{\partial x^{\beta'}}{\partial x^\beta}\frac{\partial x^\gamma}{\partial x^{\gamma'}}\ldots\frac{\partial x^\delta}{\partial x^{\delta'}} T^{\alpha\ldots\beta}{}_{\gamma\ldots\delta} \tag{2.9}$$

is defined as a *tensor* of type $(n, m)$ under a coordinate transformation, where the integers *n* and *m* are the number of superscripts and subscripts, respectively. It is important to note that the order of the indices is important, as any difference in its order would result to a whole different tensor. With this definition, we notice that vectors and dual vectors are just a tensor of type $(1, 0)$ and $(0, 1)$, respectively.

We introduce a special tensor called the *metric tensor* $g_{\alpha\beta}$ which represents the gravitational field in a specific space-time. The metric tensor is symmetric, i.e., $g_{\alpha\beta} = g_{\beta\alpha}$, and is used to describe the inner product between two vectors: $g_{\alpha\beta} u^\alpha u^\beta$.

The metric can be used to lower and raise indices. For instance,

$$A_\alpha = g_{\alpha\beta}A^\beta \qquad \text{(Index raising)} \tag{2.10}$$

$$B^\alpha = g^{\alpha\beta}B_\beta \qquad \text{(Index lowering)} \tag{2.11}$$

where $g^{\alpha\beta}$ is the inverse of the metric tensor such that

$$g^{\alpha\beta}g_{\alpha\beta} = \delta^\alpha_\beta \tag{2.12}$$

Tensors are not embedded on the manifold itself. Tensors, like vectors, are always projected to be tangent to the manifold at any point $P$. They are defined in a plane tangent to the manifold at that point; the plane is called a *tangent plane* at $P$. Therefore, tensors at point $P$ can be added and contracted, resulting to a different tensor. However, a tensor at $P$ and another at $Q$ cannot be combined tensorially because they don't exist in the same tangent plane. Consider for example a tensor $A^\alpha$ at $P$ and $B^\alpha$ at $Q$. The corresponding operations $A^\alpha(P)B^\alpha(Q)$ and $A^\alpha(Q) - A^\alpha(P)$ are not considered as tensorial operations. This shows that differentiation is not a straightforward operation on tensors. We use some kind of rule to transport a tensor from one tangent plane to another.

### 2.1.3 Covariant Derivatives

Consider a curve $\gamma$ with its tangent vector $u^\alpha$, and a vector field $A^\alpha$ in its neighborhood. Given that points $P$ and $Q$ have coordinates $x^\alpha$ and $x^\alpha + dx^\alpha$, respectively, the differentiation from the previous section becomes

$$dA^\alpha \equiv A^\alpha(Q) - A^\alpha(P) \tag{2.13}$$

$$= A^\alpha(x^\alpha + dx^\alpha) - A^\alpha(x^\alpha) \tag{2.14}$$

$$= A^\alpha{}_{,\beta}dx^\beta \tag{2.15}$$

We let the previous operation undergo a coordinate transformation to show that the above operation isn't tensorial.

$$A^{\alpha'}{}_{,\beta'} = \frac{\partial}{\partial x^{\beta'}}A^{\alpha'} \tag{2.16}$$

$$= \frac{\partial}{\partial x^{\beta'}}\left(\frac{\partial x^{\alpha'}}{\partial x^\alpha}A^\alpha\right) \tag{2.17}$$

$$= \frac{\partial x^\beta}{\partial x^{\beta'}}\frac{\partial}{\partial x^\beta}\left(\frac{\partial x^{\alpha'}}{\partial x^\alpha}A^\alpha\right) \tag{2.18}$$

$$= \frac{\partial x^{\alpha'}}{\partial x^\alpha}\frac{\partial x^\beta}{\partial x^{\beta'}}A^\alpha{}_{,\beta} + \frac{\partial^2 x^{\alpha'}}{\partial x^\alpha \partial x^\beta}\frac{\partial x^\beta}{\partial x^{\beta'}}A^\alpha \tag{2.19}$$

To be tensorial, the derivative operator should be in the form

$$DA^\alpha = A^\alpha_{\mathrm{T}}(Q \to P) - A^\alpha(P) \tag{2.20}$$

where $A^\alpha_{\mathrm{T}}(Q \to P)$ is the resulting vector when $A^\alpha$ is transported from $Q$ to $P$. By and identity value of $A^\alpha(Q) - A^\alpha(Q)$, the tensorial operator would simplify into

$$DA^\alpha = (A^\alpha(Q) - A^\alpha(P)) + (A^\alpha_{\mathrm{T}}(Q \to P) - A^\alpha(Q)) \tag{2.21}$$

$$DA^\alpha = dA^\alpha + \delta A^\alpha \tag{2.22}$$

where $\delta A^\alpha = A^\alpha_{\mathrm{T}}(Q \to P) - A^\alpha(Q)$ is not a tensorial operator. We introduce a non-tensorial field ${\Gamma^\alpha}_{\mu\beta}$ called *connection* that shows that $\delta A^\alpha$ is linear both in $A^\mu$ and $dx^\beta$, such that $\delta A^\alpha = {\Gamma^\alpha}_{\mu\beta} A^\mu dx^\beta$. Plugging this in to Eqn. (2.22),

$$DA^\alpha = dA^\alpha + {\Gamma^\alpha}_{\mu\beta} A^\mu dx^\beta \tag{2.23}$$

$$DA^\alpha = {A^\alpha}_{,\beta} dx^\beta + {\Gamma^\alpha}_{\mu\beta} A^\mu dx^\beta \tag{2.24}$$

We divide this by the increment in the curve's parameter $d\lambda$.

$$\frac{DA^\alpha}{d\lambda} = {A^\alpha}_{;\beta} u^\beta \tag{2.25}$$

where $u^\beta = dx^\beta/d\lambda$ is the tangent vector, while

$${A^\alpha}_{;\beta} \equiv {A^\alpha}_{,\beta} + {\Gamma^\alpha}_{\mu\beta} A^\mu \tag{2.26}$$

This is called the *covariant derivative* of vector $A^\alpha$. The covariant derivative can be also presented in other notations such as ${A^\alpha}_{;\beta} \equiv \nabla_\beta A^\alpha$ and $DA^\alpha/d \equiv \nabla_u A^\alpha$.

Since ${A^\alpha}_{;\beta}$ is a tensor of type $(1,1)$, we can extrapolate the transformation property of the connection factor. We start with ${\Gamma^\alpha}_{\mu\beta} A^\mu = {A^\alpha}_{;\beta} - {A^\alpha}_{,\beta}$ from Eqn. (2.26) and let it undergo a coordinate transform as done above.

$${\Gamma^{\alpha'}}_{\mu'\beta'} A^{\mu'} = \frac{\partial x^{\alpha'}}{\partial x^\alpha} \frac{\partial x^\beta}{\partial x^{\beta'}} {\Gamma^\alpha}_{\mu\beta} A^\mu - \frac{\partial^2 x^{\alpha'}}{\partial x^\alpha \partial x^\beta} \frac{\partial x^\beta}{\partial x^{\beta'}} A^\mu \tag{2.27}$$

Writing $A^{\mu'}$ in terms of $A^\mu$ and cancelling the $A^\mu$ on both sides, we get

$${\Gamma^{\alpha'}}_{\mu'\beta'} \frac{\partial x^{\mu'}}{\partial x^\mu} = \frac{\partial x^{\alpha'}}{\partial x^\alpha} \frac{\partial x^\beta}{\partial x^{\beta'}} {\Gamma^\alpha}_{\mu\beta} - \frac{\partial^2 x^{\alpha'}}{\partial x^\alpha \partial x^\beta} \frac{\partial x^\beta}{\partial x^{\beta'}} \tag{2.28}$$

Isolating ${\Gamma^{\alpha'}}_{\mu'\beta'}$ by multiplying $\frac{\partial x^\mu}{\partial x^{\mu'}} =$ on both sides, we get

$${\Gamma^{\alpha'}}_{\mu'\beta'} = \frac{\partial x^{\alpha'}}{\partial x^\alpha} \frac{\partial x^\beta}{\partial x^{\beta'}} \frac{\partial x^\mu}{\partial x^{\mu'}} {\Gamma^\alpha}_{\mu\beta} - \frac{\partial^2 x^{\alpha'}}{\partial x^\alpha \partial x^\beta} \frac{\partial x^\beta}{\partial x^{\beta'}} \frac{\partial x^\mu}{\partial x^{\mu'}} \tag{2.29}$$

We can extend covariant differentiation to other types of tensors. For example, we can apply this to a dual vector and obtain

$$\frac{Dp^{\alpha}}{d\lambda} = p_{\alpha;\beta}u^{\beta} \tag{2.30}$$

where

$$p_{\alpha;\beta} \equiv p_{\alpha,\beta} - \Gamma^{\mu}{}_{\alpha\beta}p_{\mu} \tag{2.31}$$

We can further extend this to any tensors of type $(m, n)$.

$$\begin{aligned} T^{m_1\ldots m}{}_{n_1\ldots n;\eta} =& T^{m_1\ldots m}{}_{n_1\ldots n,} \\ &+ \left(\Gamma^{m_1}{}_{\mu\eta}T^{\mu\ldots m}{}_{n_1\ldots n} + \ldots + \Gamma^{m}{}_{\mu\eta}T^{m_1\ldots\mu}{}_{n_1\ldots n}\right) \\ &- \left(\Gamma^{\mu}{}_{n_1\eta}T^{m_1\ldots m}{}_{\mu\ldots n} + \ldots + \Gamma^{\mu}{}_{n\eta}T^{m_1\ldots m}{}_{n_1\ldots\mu}\right) \end{aligned} \tag{2.32}$$

There is a connection term for each tensorial index with a plus sign for a superscript index and a minus sign for a subscript index.

In general relativity, due to Einstein's principle of equivalence, the connection is forced to have both *symmetric* and *metric compatible* properties.

$$\Gamma^{\alpha}{}_{\beta\gamma} = \Gamma^{\alpha}{}_{\gamma\beta} \qquad\qquad g_{\alpha\beta;\gamma} = 0 \tag{2.33}$$

The connection that satisfies these properties is determined by a metric

$$\Gamma^{\alpha}{}_{\beta\gamma} = \frac{1}{2}g^{\mu\beta}(g_{\mu\beta,\gamma} + g_{\mu\gamma,\beta} - g_{\beta\gamma,\mu}) \tag{2.34}$$

where $\Gamma^{\alpha}{}_{\beta\gamma}$ in this context is called the *Christoffel symbol*, which connects the Einstein equation.

To end, if the covariant derivative of a tensor field along a curve $\gamma$ vanishes, the tensor field is said to be *parallel transported* along the curve.

### 2.1.4 Geodesics

Consider the same curve $\gamma$ described by the parametrization $x^{\alpha}(\lambda)$, where $\lambda$ is an arbitrary parameter. Therefore, the distance between two points $P$ and $Q$ along the curve is given by

$$\Delta x = \int_P^Q ds = \int_P^Q \frac{ds}{d\lambda}d\lambda \tag{2.35}$$

Since,

$$ds^2 = dx^{\mu}dx_{\mu} = g_{\mu\nu}dx^{\mu}dx^{\nu}$$

$$ds = \sqrt{\pm g_{\mu\nu} dx^\mu dx^\nu} \tag{2.36}$$

The distance between the two points becomes

$$\Delta x = \int_P^Q \sqrt{\pm g_{\mu\nu} dx^\mu dx^\nu} d\lambda \tag{2.37}$$

where $\dot{x^\mu} \equiv dx^\mu/d\lambda$. In the square root, the positive sign is assigned if the curve is spacelike. Meanwhile, the negative sign is assigned if the curve is timelike. Additionally, it is known that the curve is nowhere null and that is invariant under a reparametrization, $\lambda \to \lambda'(\lambda)$.

The curve is considered *geodesic* if it extremizes the distance between points $P$ and $Q$. Meanwhile, the distance $\Delta x$ is an extremum if it satisfies the Euler-Lagrange equations

$$\frac{d}{d\lambda}\left(\frac{\partial \mathcal{L}}{\partial \dot{x^\alpha}}\right) - \frac{\partial \mathcal{L}}{\partial x^\alpha} = 0 \tag{2.38}$$

where $\mathcal{L} = \sqrt{\pm g_{\mu\nu} dx^\mu dx^\nu}$ is the Lagrangian, $\mathcal{L}' = \frac{1}{2} g_{\alpha,\beta} \dot{x^\alpha} \dot{x^\beta}$ is the derivative of the Lagrangian, and the dot denotes the derivative of the vector with respect to $\lambda$.
This just signifies that $x^\alpha(\lambda)$ must satisfy the differential equation

$$\ddot{x^\alpha} + \Gamma^\alpha{}_{\beta\gamma} \dot{x^\gamma} \dot{x^\beta} = \kappa(\lambda) \dot{x^\alpha} \tag{2.39}$$

$$\frac{d\dot{x^\alpha}}{dx^\beta} \dot{x^\beta} + \Gamma^\alpha{}_{\beta\gamma} \dot{x^\gamma} \dot{x^\beta} = \kappa(\lambda) \dot{x^\alpha} \tag{2.40}$$

$$u^\beta (u^\alpha{}_{,\beta} + \Gamma^\alpha{}_{\beta\gamma} u^\gamma) = \kappa(\lambda) \dot{x^\alpha} \tag{2.41}$$

$$u^\alpha{}_{;\beta} u^\beta \kappa(\lambda) \dot{x^\alpha} \tag{2.42}$$

where $\kappa(\lambda) = d(ln\mathcal{L})/d\lambda$. The equation is called the *geodesic equation*.

If the geodesic is either timelike or spacelike, we have

$$d\tau^2 = - g_{\alpha\beta} dx^\alpha dx^\beta \tag{2.43}$$

$$ds^2 = g_{\alpha\beta} dx^\alpha dx^\beta \tag{2.44}$$

respectively, where $\tau$ is the proper time and $s$ is the proper distance. If we use these as our parameters in the timelike and spacelike geodesics, respectively, we get a lagrangian value $\mathcal{L} = 1$. The geodesic equation becomes

$$u^\alpha{}_{;\beta} u^\beta = u^\alpha \frac{d}{d\lambda}(ln1) = 0 \tag{2.45}$$

this is the geodesic equation for a curve which is affinely parametrized. Parameters related to the proper time and proper distance is called *affine parameters*.

Along a affinely parametrized geodesic, the scalar quantity $\epsilon = u^\alpha u_\alpha$ is constant.

$$\frac{d\epsilon}{d\lambda} = \frac{D\epsilon}{d\lambda} = (u^\alpha u_\alpha)_{;\beta} u^\beta \tag{2.46}$$

$$= (u^\alpha{}_{;\beta} u^\beta) u_\alpha + u^\alpha (u_{\alpha;\beta} u^\beta) \tag{2.47}$$

With the use of Equation. $((2.45))$, we have

$$\frac{d\epsilon}{d\lambda} = 0 \tag{2.48}$$

where the constant $\epsilon$ changes per chosen parameter $\lambda$ along the geodesic:

$$\epsilon = \begin{cases} -1 & \text{timelike} \\ +1 & \text{spacelike} \\ 0 & \text{null} \end{cases} \tag{2.49}$$

## 2.2 The Alcubierre warp drive

As we discussed earlier, we can introduce an apparent expansion of space-time that would essentially "push" us away from a point $A$ at an arbitrary large speed. At the same time, we can utilize a corresponding contraction of space-time to essentially "pull" us to a different location, point $B$, with the same amount of speed as the expansion. This is the genius concept underlying the Alcubierre warp drive. We wish to create a local curvature in space-time that will essentially "push" and "pull" a spaceship through two far away regions in space, making it seem like it is moving faster than the speed of light.

We shall introduce a space-time metric that would satisfy the characteristics described above

$$ds^2 = g_{\alpha\beta} dx^\alpha dx^\beta \tag{2.50}$$

$$= -(\alpha^2 - \beta_i \beta^i) dt^2 + 2\beta_i dx^i dt + \gamma_{ij} dx^i dx^j \tag{2.51}$$

wherein $\gamma_{ij}$ is the 3-metric of the constant-$t$ hypersurfaces, $\alpha$ is a lapse function that gives the interval of the proper time between nearby hypersurfaces measured by an "Eulerian" observer - an observer whose 4-momentum is normal to the hypersurface - and $\beta^i$ relates the spatial coordinate system on the different hypersurfaces.

If we consider, for example, a space ship moving along the positive $x$-axis direction of a cartesian coordinate system. We find that the specific space-time metric

that our space ship should ride to be set in motion in the trajectory described by the Alcubierre warp distortion is described by the arbitrary function of time, $x_s(t)$. This specific metric would have the following values:

$$\alpha = 1 \tag{2.52}$$

$$\beta^x = -v_s(t)f(r_s(t)) \tag{2.53}$$

$$\beta^y = \beta^z = 0 \tag{2.54}$$

$$\gamma_{ij} = \delta_{ij} \tag{2.55}$$

where:

$$v_s(t) = \frac{dx_s(t)}{dt} \tag{2.56}$$

and

$$r_s(t) = \sqrt{(x - x_s(t))^2 + y^2 + z^2} \tag{2.57}$$

where Eqns. ((2.56))and ((2.57)) would describe how our warp-drive distortion is moving with our space ship in space-time. The center or the bridge of the warp bubble is given by the $r_s(t)$ and follows the trajectory described by a function of the time, $(x_s(t), 0, 0)$. On the other hand, $v_s(t)$, describes the rate of change in the trajectory of the center of the warp bubble with respect to time. We call this parameter the *warp speed* or *velocity* of the Alcubierre warp drive. Essentially, a spaceship that rides in the bridge of the warp bubble with a corresponding warp speed greater than the speed of light, would experience FTL travel from an observer at infinity. It is important to note that in the duration of this manuscript, we shall use a constant value for the warp speed value, $v$.

We also use Miguel Alcubierre's choice for the function $f$

$$f(r_s) = \frac{\tanh(\sigma(r_s + R)) - \tanh(\sigma(r_s - R))}{2\tanh(\sigma R)} \tag{2.58}$$

where $R$ is the radius of the warp bubble and $\sigma$ is the width or thickness of the warp bubble. Notice that for large values of $\sigma$ the function $f(r)$ approaches what we call a "top hat" function:

$$f(r_s) = \begin{cases} 1 & r_s \in [-R, R] \\ 0 & \text{otherwise} \end{cases} \tag{2.59}$$

With the following definitions, the metric (2.51) can be rewritten as:

$$ds^2 = -dt^2 + (dx - v_s f(r_s)dt)^2 + dy^2 + dz^2 \tag{2.60}$$

The values from the previous expressions give us a deeper understanding of this space-time geometry. First, we see from Eq.(2.60) that the 3-geometry of the hypersurfaces is always flat. Second, we see that the fact that the lapse function is given by $\alpha = 1$ implies that the time-like curves normal to the hypersurfaces are geodesics, meaning that the Eulerian observers are experiencing free fall. Lastly, when the value of v approaches zero, the metric would simplify into flat space or Minkowski metric.

Similarly when we move outside the vicinity of the warp-drive there would be a steep transition into flat space as described by the top hat function (2.59) and as shown in Fig. (2.1) for different values of $\sigma$. We see that any time $t$ space-time will be flat everywhere except for the warp drive vicinity centered around $(x_s(t), 0, 0)$ with a radius of $R$. It is important to note that as you increase the value of $\sigma$, the steepness of change in values as you move further away from the warp bubble also increases. Meanwhile, if you decrease the value of $\sigma$, the function would show a more relaxed change in values.

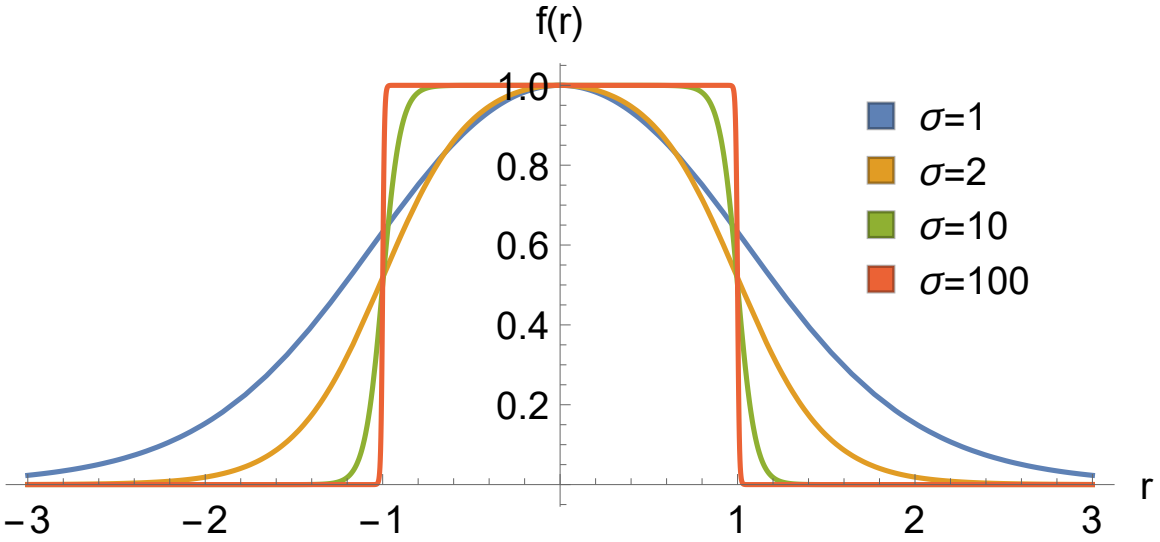


Figure 2.1: The Alcubierre shape function $f(r)$ for different values of the width bubble $\sigma$ as the distance from the center of the warp bubble is increased. We considered the following values: $\sigma \in \{1, 2, 10, 100\}$. Notice that as we increase the values for $\sigma$ we get a more steep change in values while for smaller values of $\sigma$ we get a more relaxed change in values

## 2.3 Round trip using the Alcubierre warp drive

To discuss more clearly how this unique space-time permits FTL travel, we consider as an example a spaceship's travel between two different points in space as described in Fig. (2.2). We shall call the starting and end points of our travel as point $A$ and point $B$. Point $A$ and point $B$ are separated by a distance $D$ in flat space. An Alcubierre warp drive emerges in between this two points starting from a distance $d$ from point $A$ and ending at a distance $d$ from point $B$. We consider time $t_0 = 0$ where the spaceship would start travelling from point $A$ to point $B$ with a speed of $v \ll 1$ using its rocket technology. After reaching a distance $d$ from point $A$, the spaceship stops as it would start interacting with the warp bubble centered on its current location with a radius of $R$. We assume the following inequality of distances given below.

$$R \ll d \ll D \tag{2.61}$$

The space-time distortion would move in such a way that the spaceship is pushed away from point $A$ with a coordinate acceleration that increases rapidly from 0 to a constant value $a$. Since our spaceship is at rest at the center of the warp bubble, the distortion would develop smoothly form flat space as described by Eq. (2.60).

When the space ship is midway between $A$ and $B$, the distortion is modified in such a way that the coordinate acceleration changes instantaneously from $a$ to $-a$. Since the coordinate acceleration at the second part of the trip is set to be the opposite of the coordinate acceleration at the first part of the trip, the spaceship is will find itself eventually at rest the same distance $d$ from point $B$. At this point the warp drive distortion would disappear and the spaceship would be back on flat space. The trip is then completed by travelling the same speed $v$ to reach point $B$

If there is really an instantaneous change in coordinate acceleration as discussed above, the total coordinate time $T$ elapsed in one way trip from point $A$ to $B$.

$$T = 2\left(\frac{d}{v} + \sqrt{\frac{D-2d}{a}}\right) \tag{2.62}$$

Since point $A$ and $B$ are located in flat space, their proper time is equal to the coordinate time. Meanwhile, the proper time measured on the spaceship is given by:

$$T = 2\left(\frac{d}{\gamma v} + \sqrt{\frac{D-2d}{a}}\right) \tag{2.63}$$

where $\gamma$ is given by

$$\gamma = (1 - v^2)^{-1/2} \tag{2.64}$$

We then observe that the time dilation comes only from the initial and final stages of the trip, when the spaceship is required to use its engine to travel through flat space. Since we considered earlier that $d \ll D$, the time elapse could be simplified into

$$\tau = T = 2\sqrt{\frac{D}{a}} \tag{2.65}$$

Notice that we can continue to minimize the elapsed proper time on the trip by increasing the coordinate acceleration $a$ caused by the warp drive distortion. We can also complete a round trip back to point $A$ and since it would only take twice as long, travel time would be arbitrarily small both to the point of view of an observer in the spaceship and an observer in locations $A$ and $B$. Essentially the spaceship will be able to travel much faster than the speed of light. At the same time, as mentioned earlier, the spaceship will always remain in a time-like trajectory as light is also distorted by the warp drive curvature.

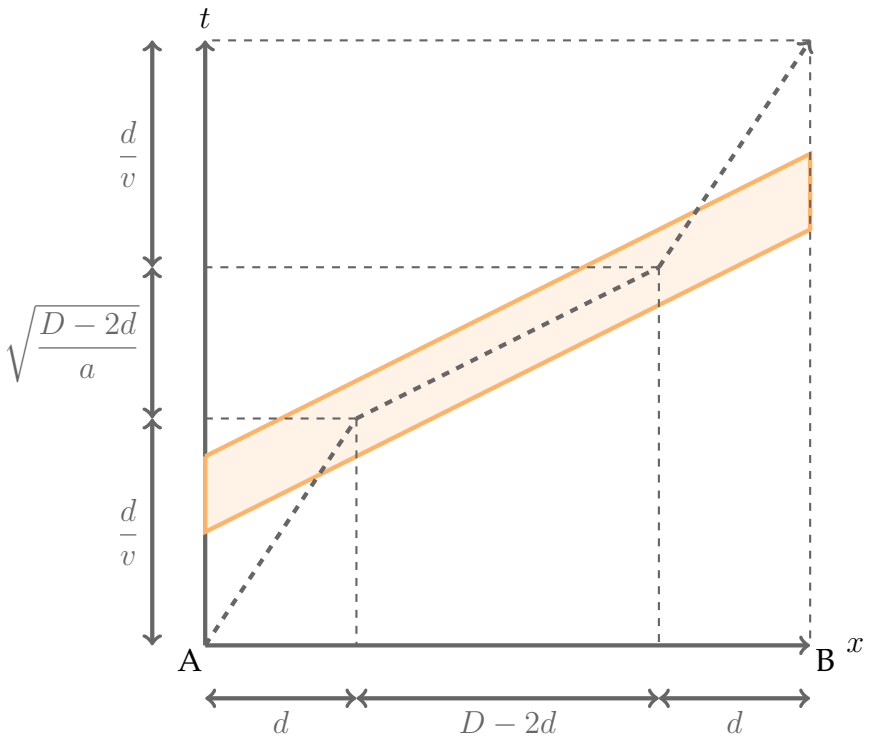


Figure 2.2: World line of a spaceship's travel from point A to point B while riding an Alcubierre warp drive depicted by the color orange band.

# Chapter 3

# Photon trajectories in the Alcubierre wrap drive

In this calculation we visualize the ray trajectories of photon beams in the Alcubierre warp drive metric. We do this by solving for the geodesic equations in an Alcubierre warp drive distortion and solving for the solutions of the coupled ordinary differential equations (ODE) that comes with it. The warp speed and warp bubble width given by $v$ and $\sigma$, respectively, are then varied to study its effects on the ray trajectories and deflection angle. To do this we must begin with considering the Alcubierre warp drive metric (2.60) that we discussed in Chapter 2.

$$ds^2 = -dt^2 + (dx - v_s f(r_s)dt)^2 + dy^2 + dz^2 \tag{3.1}$$

The Alcubierre warp drive metric can easily be written in matrix form. The warp drive metric is important because we use the metric and inverse metric to solve for the Christoffel symbols that is important in solving for the geodesic equations. In this form we see,

$$g_{\mu\nu} = \begin{pmatrix} v_s^2 f(r_s)^2 - 1 & -v_s f(r_s) & 0 & 0 \\ -v_s f(r_s) & 1 & 0 & 0 \\ 0 & 0 & 1 & 0 \\ 0 & 0 & 0 & 1 \end{pmatrix} \tag{3.2}$$

and

$$g^{\mu\nu} = \begin{pmatrix} -1 & -v_s f(r_s) & 0 & 0 \\ -v_s f(r_s) & 1 - v_s^2 f(r_s)^2 & 0 & 0 \\ 0 & 0 & 1 & 0 \\ 0 & 0 & 0 & 1 \end{pmatrix} \tag{3.3}$$

Now that we have the Alcubierre warp drive metric, we now can solve for the Christoffel symbols. The Christoffel symbols is given by

$$\Gamma^{\alpha}_{\mu\nu} = \frac{1}{2} g^{\alpha\delta} \left( \frac{\partial g_{\delta\mu}}{\partial x^{\nu}} + \frac{\partial g_{\delta\nu}}{\partial x^{\mu}} - \frac{\partial g_{\mu\nu}}{\partial x^{\delta}} \right) \tag{3.4}$$

Evaluating the Christoffel symbols for the Alcubierre warp drive metric, we get the following values,

$$\Gamma^{t}_{tt} = f^2 f_x v_s^3 \qquad \Gamma^{y}_{tt} = -f f_y v_s^2 \tag{3.5}$$

$$\Gamma^{z}_{tt} = -f f_z v_s^2 \tag{3.6}$$

$$\Gamma^{x}_{tt} = f^3 f_x v^4 - f f_x v^2 - f_t v - \partial_t v \tag{3.7}$$

$$\Gamma^{t}_{tx} = -f f_x v^2 \qquad \Gamma^{x}_{tx} = -f^2 f_x v^3 \tag{3.8}$$

$$\Gamma^{y}_{tx} = \frac{f_y v}{2} \qquad \Gamma^{z}_{tx} = \frac{f_z v}{2} \tag{3.9}$$

$$\Gamma^{t}_{ty} = -\frac{f f_y v^2}{2} \qquad \Gamma^{x}_{ty} = -\frac{f^2 f_y v^3 + f_y v}{2} \tag{3.10}$$

$$\Gamma^{t}_{tz} = -\frac{f f_z v^2}{2} \qquad \Gamma^{x}_{tz} = -\frac{f^2 f_z v^3 + f_z v}{2} \tag{3.11}$$

$$\Gamma^{t}_{xx} = f_x v \qquad \Gamma^{x}_{xx} = f f_x v^2 \tag{3.12}$$

$$\Gamma^{t}_{xy} = \frac{f_y v}{2} \qquad \Gamma^{x}_{xy} = \frac{f f_y v^2}{2} \tag{3.13}$$

$$\Gamma^{t}_{xz} = \frac{f_z v}{2} \qquad \Gamma^{x}_{xz} = \frac{f f_z v^2}{2} \tag{3.14}$$

with the following derivatives

$$f_t = \frac{df(r_s)}{dt} = \frac{-v_s \left(x - x_s(t)\right)}{r} \frac{df(r)}{dr} \tag{3.15}$$

$$f_x = \frac{df(r_s)}{dt} = \frac{\left(x - x_s(t)\right)}{r} \frac{df(r)}{dr} \tag{3.16}$$

$$f_y = \frac{df(r_s)}{dy} = \frac{y}{r} \frac{df(r)}{dr} \tag{3.17}$$

$$f_z = \frac{df(r_s)}{dt} = \frac{z}{r} \frac{df(r)}{dr} \tag{3.18}$$

where

$$\frac{df(r_s)}{dr} = \frac{\sigma[\operatorname{sech}^2\left(\sigma(r+R)\right) - \operatorname{sech}^2\left(\sigma(r-R)\right)]}{2\tanh(\sigma R)} \tag{3.19}$$

We learned in Chapter II that the geodesic equations dictate how a massless particle would freely fall around a space-time curvature. The geodesic equations contain information on a particle's trajectories and momenta. We recall that it is given by

$$\frac{dp^{\alpha}}{d\lambda} + \Gamma^{\alpha}_{\mu\nu} p^{\mu} p^{\nu} = 0 \tag{3.20}$$

Using the Christoffel symbols that we solved, we can then solve for the geodesic equations for the Alcubierre warp drive.

$$\frac{dp^t}{d\lambda} + \Gamma^t_{tt}(p^t)^2 + \Gamma^t_{xx}(p^x)^2 + 2\Gamma^t_{tx}p^tp^x + 2\Gamma^t_{ty}p^tp^y + 2\Gamma^t_{xy}p^xp^y + 2\Gamma^t_{xz}p^xp^z + 2\Gamma^t_{tz}p^tp^z = 0 \quad (3.21)$$

$$\frac{dp^x}{d\lambda} + \Gamma^x_{tt}(p^t)^2 + \Gamma^x_{xx}(p^x)^2 + 2\Gamma^x_{tx}p^tp^x + 2\Gamma^x_{ty}p^tp^y + 2\Gamma^x_{xy}p^xp^y + 2\Gamma^x_{xz}p^xp^z + 2\Gamma^x_{tz}p^tp^z = 0 \quad (3.22)$$

$$\frac{dp^y}{d\lambda} + \Gamma^y_{tt}(p^t)^2 + 2\Gamma^y_{tx}p^tp^x = 0 \quad (3.23)$$

$$\frac{dp^z}{d\lambda} + \Gamma^z_{tt}(p^t)^2 + 2\Gamma^z_{tx}p^tp^x = 0 \quad (3.24)$$

where $\lambda$ is just an arbitrary variable that we will use in this calculation.

If we restrict our warp bubble to only travel along the $x$-axis, our system would be simplified due to the cylindrical symmetry about the said axis. This entails that the $p^z$ component of the photon four-momentum along with the $z$-trajectory would be equal to zero. The geodesic equations would then be reduced into three equations due to this restriction.

$$\frac{dp^t}{d\lambda} + \Gamma^t_{tt}(p^t)^2 + \Gamma^t_{xx}(p^x)^2 + 2\Gamma^t_{tx}p^tp^x + 2\Gamma^t_{ty}p^tp^y + 2\Gamma^t_{xy}p^xp^y = 0 \quad (3.25)$$

$$\frac{dp^x}{d\lambda} + \Gamma^x_{tt}(p^t)^2 + \Gamma^x_{xx}(p^x)^2 + 2\Gamma^x_{tx}p^tp^x + 2\Gamma^x_{ty}p^tp^y + 2\Gamma^x_{xy}p^xp^y = 0 \quad (3.26)$$

$$\frac{dp^y}{d\lambda} + \Gamma^y_{tt}(p^t)^2 + 2\Gamma^y_{tx}p^tp^x = 0 \quad (3.27)$$

As discussed earlier, in this manuscript we only consider the steady-state problem where the warp speeds of our Alcubierre bubble is constant, so that $v_s = v =$ constant, and $x_s = vt$, where $v$ is our warp speed. It is important to note that to better observe the photon scattering for different impact parameters, we set the radius of the warp bubble to be $R = 3$.

We then complete the set of nonlinear coupled ordinary differential equations by introducing the momenta-trajectory relations

$$p^t = \frac{dt}{d\lambda} \quad (3.28)$$

$$p^x = \frac{dx}{d\lambda} \quad (3.29)$$

and

$$p^y = \frac{dy}{d\lambda} \tag{3.30}$$

These equations are important because it gives us information about the changes in energy of the photon as it traverses the vicinity of the warp bubble. This information, along with the overall blue-shift of photon energy, will be further discussed in Chapter V.

We then introduce our initial system wherein a beam of light is shone to an incoming Alcubierre warp drive from a position outside the vicinity of the warp drive distortion. We consider an Alcubierre warp bubble moving with a velocity $v$ in the negative $x$-direction. Meanwhile the beam of photons are initially released from the negative infinity moving in the positive $x$- direction to arrive and propagate through the distortion. The initial setup is shown in Fig. (3.1).

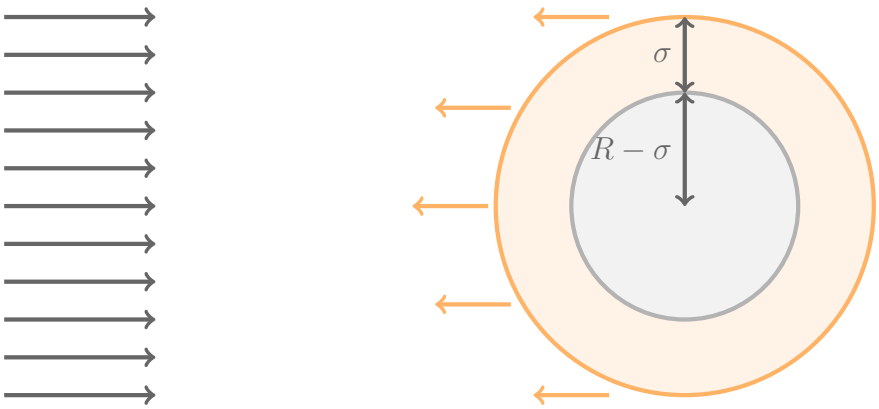


Figure 3.1: Light or photons starting from spatial infinity collide and propagate through an Alcubierre warp drive distortion of bubble thickness $\sigma$ and radius $R$. The resulting light trajectories will then be studied.

The nonlinear coupled differential equation composed of the geodesic equations, Eqns. (3.25 - 3.27), and the momenta-trajectory relations, Eqns. (3.28-3.30) , will be numerically integrated to yield equations representing the $t$-,$x$-,$y$- component trajectories and momenta of the photon propagation. The trajectories and angular deflections of light will be discussed in Chapter IV, while the energy shifts and overall blue-shift of light will be discussed in Chapter V, as mentioned above. We shall consider different values of the warp speed and warp bubble width for these results.

We consider the following initial values for our system:

$$t(0) = 0 \qquad p^t(0) = 1 \tag{3.31}$$

$$x(0) = -20 \qquad p^x(0) = 1 \tag{3.32}$$

$$y(0) = b \qquad p^y(0) = 0 \tag{3.33}$$

We position the photons 20 light seconds away from the space ship to be certain that our probes start in flat space-time and that there is no initial interaction between the photons and the warp drive distortion. There is an initial $x$-momenta of 1 light second per increment in $\lambda$ so that we can be sure that the photons are moving towards the warp drive. Meanwhile, for the initial values of the $y$-coordinate, or what we want to call as the *impact parameter* of the photons, we consider photons equally placed in the range $-6 \leq y \leq 6$. The difference in the impact parameter values would help us understand the gravitational lensing in the warp drive. The initial $y$-momenta is set to be zero so that the photons will continue to move parallel to the $x$-axis and eventually travel through the warp drive.

As discussed earlier, the Alcubierre warp drive metric would effectively vanish when the warp speed is zero as our metric would just reduce to flat space. This means that there is no spacetime curvature for an Alcubierre warp drive with a warp velocity, $v = 0$.

## 3.1 A check of our ray tracing results

Anderson et al. in their paper [23] discussed about the ray trajectories of light for an Alcubierre warp drive space-time that was simulated by means of a Tamm medium whose properties are similar to those of a vacuum. The concept of a Tamm medium [32,33] provide opportunities in implementing classical electromagnetism formalism and facilitating corresponding analysis in general-relativistic scenarios that would otherwise be impractical or impossible to study by direct methods [34–37]. In recent years, metamaterial-based simulations of negative-phase-velocity propagation of light [38] have been proposed for different space-time metrics, such as the Schwarzschild [39], Schwarzschild-de Sitter [40], Kerr [41–44], Kerr-Newman [45], Reinssner-Nordstrom [46], cosmic string [47], and wormhole [48] space-times.

To provide the ray tracing visualization of light using this nanostructured metamaterial, the paper introduced a Lorentz transformation to eliminate the time-

dependence of the position of the warp bubble. A Hamiltonian function was then derived from the electric and magnetic fields of a photon that is set-up to interact with the Alcubierre warp bubble. The resulting coupled ODE is then solved by the *Runge-Kutta* method to yield its time-dependent relative wave vector and displacement.

We try to replicate the results of Anderson by using our Lagrangian-based geodesics to solve for the trajectories of photons inside the vicinity of the warp drive. We set our warp bubble to have a radius of $R = 1$, a warp bubble thickness of $\sigma = 5$, and a velocity $v \in \{0.3, 0.6, 0.9\}$ to see if our results check out with previously accepted results. We considered equally spaced light rays whose motion is initially parallel to the $x$-axis. The corresponding initial positions are $x(0) = -28$ and $-1.5 \leq y(0) \leq 1.5$ with an initial direction or momentum of $p^x = 1$.

We parametrized our results to show the propagation of light in the warp drive and compared our Lagrangian-based results to the results of Anderson. Our ray tracing of light is given by Figs. (3.2a - 3.2c). These results correspond to the results of Anderson and follows their observation that the light rays exhibit a focusing effect, with the focus lying on the positive $x$-axis, once it passes through the warp bubble. The focusing effect also manifest better once the warp speed value is increased, while the focus shifts towards the coordinate origin.

Another aspect of the ray tracing results that is easily observable in the original paper is that the warp bubble changes eccentricity as the warp speed is increased from the perspective of an observer at infinity. However, in our reproduced results, we didn't account for this change as this change in eccentricity usually represents special relativistic effects happening to the warp bubble. Since we are mainly concerned about the visualization of the photon trajectories in the warp bubble in this manuscript, we chose not to visualize the special relativistic effects accurately.

In the succeeding chapters we will start presenting our results for this manuscript. In Chapter IV, we will present the ray tracing of light for warp bubbles of different warp speeds and warp bubble thickness and talk about the resulting angular deflections of light in the system. In Chapter V, we will present the photon energy shifts in the warp drive and discuss it's overall blue-shifts for different values of warp speed and warp bubble thickness.

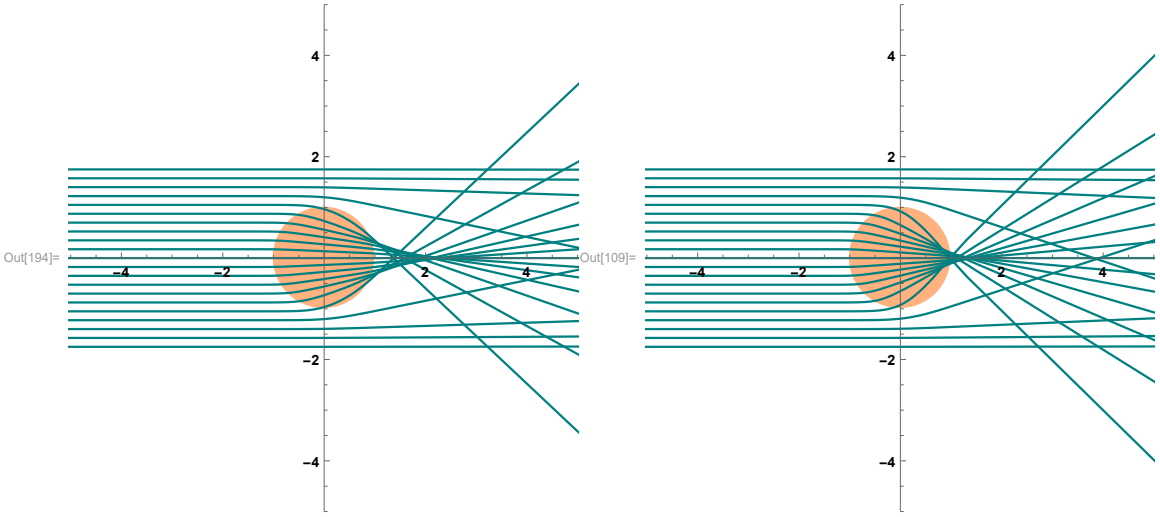


(a) Photon scattering for a warp drive with $v$=0.3(b) Photon scattering for a warp drive with $v$=0.6

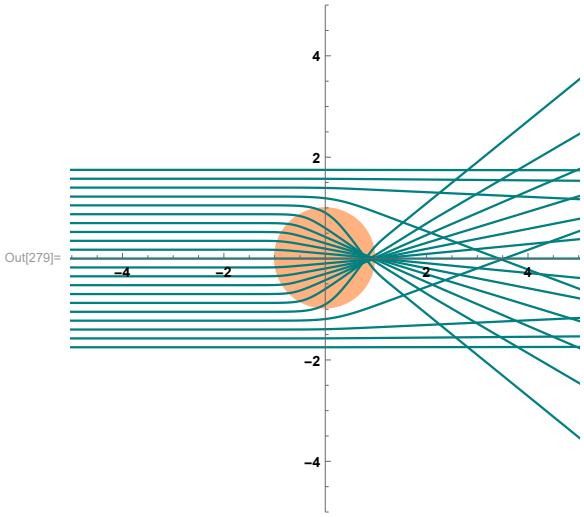


(c) Photon scattering for a warp drive with $v$=0.9

Figure 3.2: The ray tracing of light in the Alcubierre warp drive with parameters $\sigma = 5$ and $R = 3$ for warp speeds $v \in \{0.3, 0.6, 0.9\}$.

# Chapter 4

# Photon scattering in the Alcubierre warp drive

## 4.1 Photon scattering for variable warp speeds

The visualization of the ray tracing of light interacting with an Alcubierre warp drive is given by Figs. (4.1a - 4.1d), for warp drives with warp speeds $v \in \{1, 2, 5, 10\}$. The warp bubble, represented by the solid orange circle, is re-centered to the origin to better visualize the scattering of light with respect to a moving warp bubble. The parameter values used for this visualization is $R = 3$ and $\sigma = 1$.

Light experience a gravitational lensing effect after reaching the vicinity of the warp drive. For impact parameters less than or equal to the radius of the warp drive, $b \leq R$, we observe that light would experience a strong lensing effect wherein light would cross the $x$-axis axis and be deflected to the opposite region with respect to the $x$-axis. This implies that for light rays in the region of the warp bubble, there is an inverting distortion that happens. There is also an apparent focusing effect for light rays travelling inside the region of the warp bubble. This focusing effect gets closer to the origin as we increase the values of the warp speed as discussed in [23].

Meanwhile, for light rays with impact parameters greater than the radius of the warp bubble, $b > R$, we observe that light rays experience a weak lensing similar to the lensing effects we normally observe when light travels around the vicinity of other massive objects. Additionally, light rays with the same impact parameter magnitude are symmetric to each other with respect to the $x$-axis as observed from the given plots.

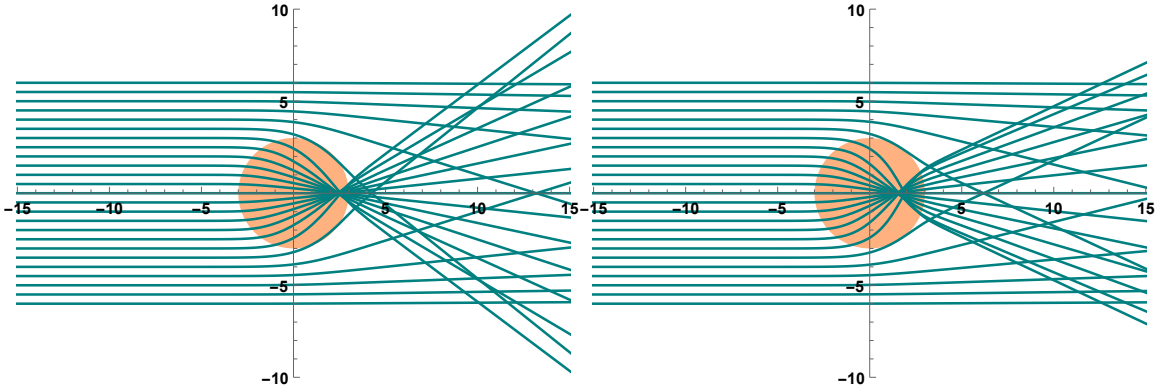


(a) Photon scattering for a warp drive with $v$=1 (b) Photon scattering for a warp drive with $v$=2

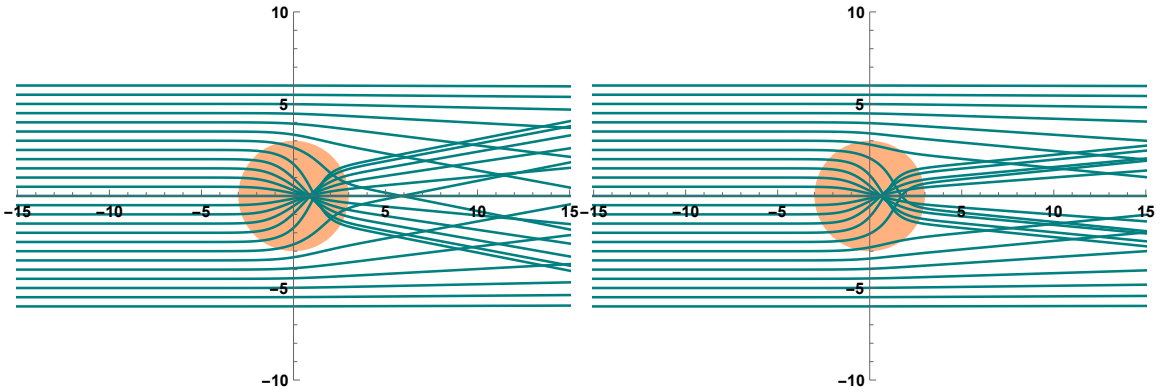


(c) Photon scattering for a warp drive with $v$=5 (d) Photon scattering for a warp drive with $v$=10

Figure 4.1: Ray trajectories for light in the $xy$-plane of the Alcubierre warp drive for warp speeds $v \in \{1, 2, 5, 10\}$. Light from infinity is shone parallel to the $x$-axis with light rays equally spaced with impact parameters ranging from -6 to 6. Parameter values: $\sigma = 1$ and $R = 1$

Light rays with impact parameter, $b = 0$ would seem to experience no apparent lensing effect as the plots above show no apparent distortion or scattering for the specified light rays. This would be further discussed in the next section of Chapter IV. However, as we would discuss in Chapter V, there would be a total blue-shift of energy for photons beamed through an Alcubierre warp drive, including light rays with impact parameter $b = 0$.

We can then take an image for example to be beamed through an Alcubierre warp drive. The lensing effects discussed would imply that for an image to be beamed towards an Alcubierre warp drive, the observed image by an observer in the rear-end of the warp bubble would have an inverting distortion for a radial area around the center of the warp bubble. Meanwhile the rest of the image would either tend to the center of the warp bubble, if the corresponding area is still in the vicinity

of the warp drive, or remain unchanged, if it's outside the vicinity of the warp drive or if the corresponding light ray propagates through the center of the warp bubble.

We then expect that as we continue to increase our warp velocities, our set of photons would collide faster with the incoming Alcubierre warp bubble. The photons would then scatter immediately to flat space after it it leaves the vicinity of the warp drive distortion. This is why it is also important to extend our previous ray tracing visualization to a scattering visualization after some discernible time, $t$, to see how scattered our initial group of photons become after an interaction with our Alcubierre warp drive distortion for different warp velocities. The photon scattering in the Alcubierre warp drive after some time, $t = 17$ light seconds, for warp speeds, $v \in \{1, 2, 5, 10\}$, is given by the Figs. (4.2a - 4.2d).

With the initial preview of our earlier visualizations from Figs. (4.1a - 4.1d), it may seem that as we increase the warp speed values, the deflections of photons on the Alcubierre warp drive distortion decreases, but as shown by Figs. (4.2a - 4.2d), it becomes more evident that it is otherwise.

With the plots that we have below, it becomes clearer that our initial expectation is true, that as we increase the warp speeds, the photons that we have set in a far away region would reach and interact with our fast moving warp drive much faster. During the photon's interaction with the warp bubble, there is an apparent change in the $p^x$ and $p^y$ that differs for different values of the warp speed. This change in the momenta is associated with the gravitational lensing effect that happens in the warp drive. For higher values of the warp speed these differences in the momentum shifts increases leading to the huge differences in scattering and angular deflection for different warp speeds. Scattering in this study would then be how far our photons would be after some time $t$. Meanwhile, the deflection angle, as we would further discuss in the next section, would be the ratio of our $y$- and $x$- momenta after some time $t$.

From the visualizations below we observe that for warp speed value, $v = 1$, after time, $t = 17$ light seconds, given by Fig. (4.2a) the beam of light would have reached the warp drive distortion but would have just began its scattering. However, for higher warp speed values such as in Figs. (4.2b - 4.2d), we could see that our photons get more scattered and reaches further away into a region of flat space as we increase the warp speed.

Additionally, there would be an apparent difference in magnification for an image shone directly into a warp drive distortion that would be dependent on two things: The location of the observer on the rear of the warp drive who would check the distorted image formed, and the warp speed of the Alcubierre warp drive distortion. Firstly, there is an increase in magnification as we move closer to infinity and further away from the warp drive and photon interaction. We expect this to happen due to the image's increased elapsed time of scattering before reaching the observer. We can clearly see this in the visualization below as when we increase the elapsed time $t$ the image would then be more scattered due to the strong lensing mechanism of the Alcubierre wrap drive.

Secondly, there is an increase in the distorted magnification of an image as we increase the warp speed, $v$, as also discussed above since an increase in warp speeds would also mean an increase in the scattering of photons and thus, an increase in the scattering of our hypothetical image.

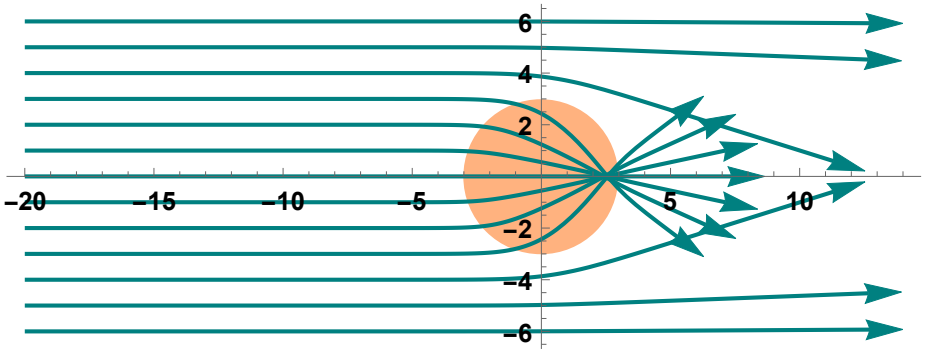


(a) Photon scattering for a warp drive with $v$=1

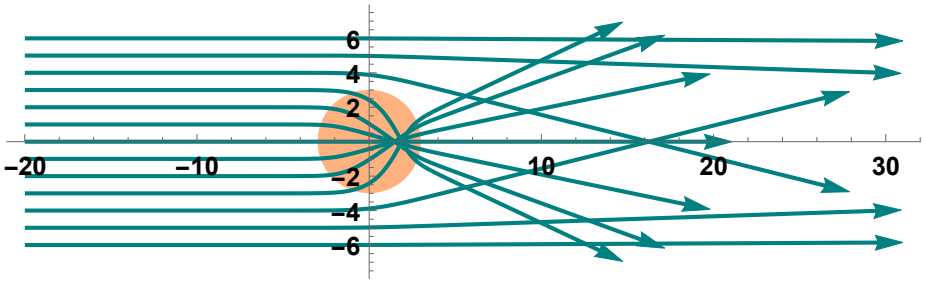


(b) Photon scattering for a warp drive with $v$=2

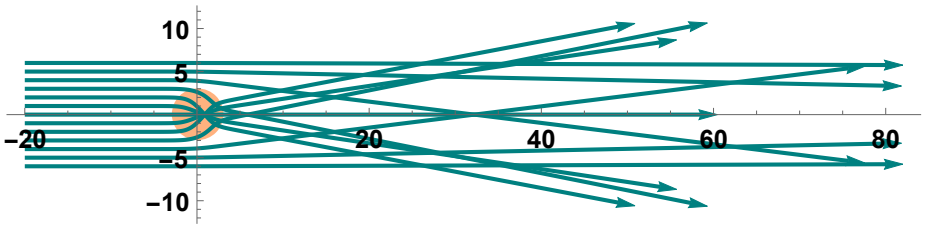


(c) Photon scattering for a warp drive with $v$=5

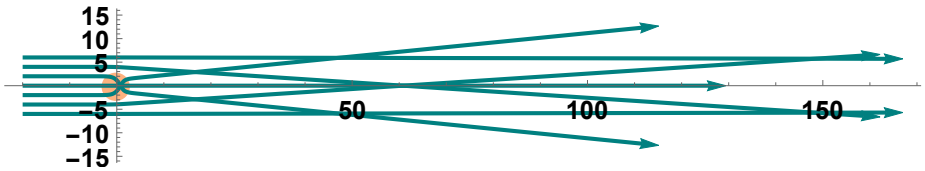


(d) Photon scattering for a warp drive with $v$=10

Figure 4.2: Ray trajectories for light in the $x7$-plane of the Alcubierre warp drive for warp speeds $v \in \{1, 2, 5, 10\}$ after time, $t = 17$ light seconds. Light from infinity is shone parallel to the $x$-axis with light rays equally spaced with impact parameters ranging from -6 to 6. Parameter values: $\sigma = 1$ and $R = 3$.

## 4.2 Deflection angles for variable warp speeds

One of our main topic of interest in this investigation are the angular deflections of photons as they interact with the Alcubierre warp drive. Following Clark et al. [49], the propagation direction of photons at infinity after they interact with the warp distortion is

$$\tan(\theta_\infty) = \frac{p^y(r=\infty)}{p^x(r=\infty)} \tag{4.1}$$

We can then compute for the inverse tangent of both sides of the equation to yield the deflection angles of photons for specific values of the impact parameter and warp speed.

To be more explicit about our definition of the deflection angles of light that has undergone distortion due to an Alcubierre warp drive, we consider Fig. (4.3). The angular deflection that we are computing for is the apparent angle formed between the momentum vector formed and the immediate $x$-axis in a local reference frame for an observer in a spatial position far away from the vicinity of the warp bubble. This is to make sure that the $p^y$ and $p^x$ momentum used in this calculation is not influenced by the warp drive distortion anymore. In this calculation we compute for the deflection angles of photons for different pairs of impact parameter and warp velocity values. We measured the deflection angles after time, $t = 100$ light seconds since the photons are already way outside of the warp bubble vicinity at that point.

For photons with impact parameter values that range from $-6 \leq b \leq 6$ that scatter in the Alcubierre warp drive with a warp bubble of radius $R = 3$, $\sigma = 1$, and warp speed values, $v \in \{1, 2, 5, 10\}$, we measure the deflection angles presented in Fig. (4.4). We observe that for the resulting deflection angles, there is a gradual increase in value for increasing magnitude values of the impact parameter reaching up to a critical impact parameter value wherein the angular deflection peaks. Meanwhile, once we consider the impact parameter values outside of this critical value, the angular deflections experience a steep descent in value rapidly reaching the value of zero once the impact parameter becomes much much greater than the warp bubble radius. This phenomena can be associated with our choice for the warp bubble width value, $\sigma$. We expect that once we increase the warp bubble width value there would be a steeper decrease in value for the deflection angles of photons with impact parameter greater than the critical impact parameter value. We would be

providing more discussions about the resulting change in photon angular deflections for variable warp bubble width values in the subsequent sections of Chapter V.

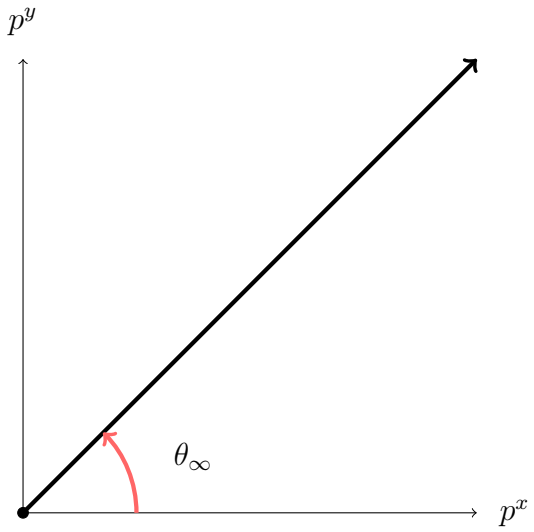


Figure 4.3: The deflection angles after photon propagation in an Alcubierre warp drive for both the strong and weak lensing is calculated by using the interaction of spatial momenta described above. The deflection angles measured would be with respect to the $x$-axis for the strong lensing mechanism and a hypothetical segment parallel to the $x$-axis for the weak lensing.

There is also an increase in the photon angular deflections as we increase the warp speed values, $v$, that reaches the asymptotic value of $\pi/2$ as the warp speed value reaches infinity. The increase in angular deflections can be related to the earlier discussion about the increase in scattering as the warp speed value is increased. It is also observed that there is a change in the peak of the angular deflection values as the warp speed is increased, wherein the impact parameter corresponding to the angular deflection's peak approaches the value, $b = 0$, as the warp speed value is increased.

Next, consider the photons that have impact parameter, $b = 0$. We observe that there wouldn't be a deflection for this special case. For these kinds of photons, $p^y = p^z = 0$, because of symmetry. Then null geodesic equations for the remaining $p^t$ and $p^x$ momentum then becomes,

$$\frac{dp^t}{d\lambda} + \Gamma^t_{tt}(p^t)^2 + \Gamma^t_{xx}(p^x)^2 + 2\Gamma^t_{tx}p^t p^x = 0 \tag{4.2}$$

and

$$\frac{dp^x}{d\lambda} + \Gamma^x_{tt}(p^t)^2 + \Gamma^x_{xx}(p^x)^2 + 2\Gamma^x_{tx}p^t p^x = 0 \tag{4.3}$$

We then consider the null normalization for the photon four momentum,

$$g_{\mu\nu}p^{\mu}p^{\nu} = 0 \tag{4.4}$$

Considering the symmetries in the $p^y$ and $p^z$ momentum, the null normalization for our system simplifies into

$$(vf-1)^2(p^t)^2 - 2vfp^tp^x + (p^x)^2 = 0 \tag{4.5}$$

From this equation we can come up with the following relation that we will use for evaluating our geodesic equation.

$$(vf-1)p^t = p^x \tag{4.6}$$

Using this relation, we can write Eqns. (4.2) and (4.3) in terms of $p^t$. The geodesic equations then simplifies into the following equations:

$$\frac{dp^t}{d\lambda} + \Gamma^t_{tt}(p^t)^2 + (vf-1)^2\Gamma^t_{xx}(p^t)^2 + 2(vf-1)\Gamma^t_{tx}(p^t)^2 = 0 \tag{4.7}$$

$$\frac{dp^x}{d\lambda} + \Gamma^x_{tt}(p^t)^2 + (vf-1)^2\Gamma^x_{xx}(p^t)^2 + 2(vf-1)\Gamma^x_{tx}(p^t)^2 = 0 \tag{4.8}$$

We can then supplying this equations with the equivalent Christoffel symbols that we solved for in Chapter III.

$$\Gamma^t_{tt} = f^2 f_x v_s^3 \qquad \Gamma^x_{tt} = f^3 f_x v^4 - f f_x v^2 - f_t v - \partial_t v \tag{4.9}$$

$$\Gamma^t_{tx} = -f f_x v^2 \qquad \Gamma^x_{tx} = -f^2 f_x v^3 \tag{4.10}$$

$$\Gamma^t_{xx} = f_x v \qquad \Gamma^x_{xx} = f f_x v^2 \tag{4.11}$$

with the following derivatives and relations

$$f_t = \frac{df(r)}{dt} = -v\left(\frac{(x-vt)}{r}\right)\left(\frac{df(r)}{dr}\right) \tag{4.12}$$

$$f_x = \frac{df(r)}{dt} = \frac{(x-vt)}{r}\left(\frac{df(r)}{dr}\right) \tag{4.13}$$

$$f_t = -vf_x \tag{4.14}$$

Eqns. (4.7) and (4.8) then simplifies to the same equations that Clark et al. [49] has discussed in their paper.

$$\frac{dp^t}{d\lambda} + vf_x(p^t)^2 = 0 \tag{4.15}$$

$$\frac{dp^x}{d\lambda} + v^2 f_x (p^t)^2 = 0 \tag{4.16}$$

We plug the equations to each other to yield a constant of motion value $p^x - vp^t = 0$, that we can use as a check to our equations of motion.

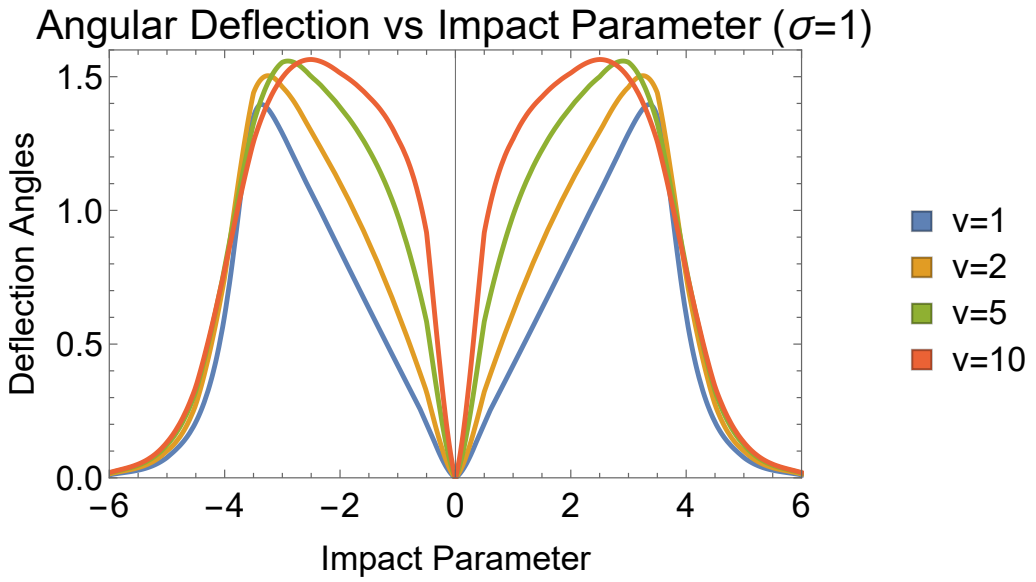


Figure 4.4: Angular deflection of photons for different impact parameter and warp speed values. Parameter values: $\sigma = 1$, and $R = 3$.

## 4.3 Photon scattering for variable warp bubble width

Most of the literature surrounding the Alcubierre warp drive metric usually leave aside discussions regarding the effect of the warp bubble width, $\sigma$, only using its effects on the discussion about the steep decrease in the $f(r)$ values as a photon leaves the radius of the warp bubble; stating that results would exhibit similar results with is no significant difference when different constant values for the warp bubble width are used. For Sections [5.3 - 5.4] and Sections [6.3 - 6.4] in Chapter V, we shall show the difference in magnitudes for the deflection angle and final energy of photons as we change the values for the warp bubble width.

We then consider the ray tracing of light in the Alcubierre wrap drive for different values of the warp bubble width. The following ray tracing given in Figs. (4.5a - 4.5c) corresponds to the bending of light in its interaction with the warp bubble distortion for warp speed values $\sigma \in \{1, 2, 5\}$, respectively. To effectively compare the following figures, we utilized the same impact parameter values, which are

equally placed along the range of $-6 \leq y \leq 6$, with the warp drive having a radius of $R = 3$, and moving with a constant speed of $v = 1$ for every case shown.

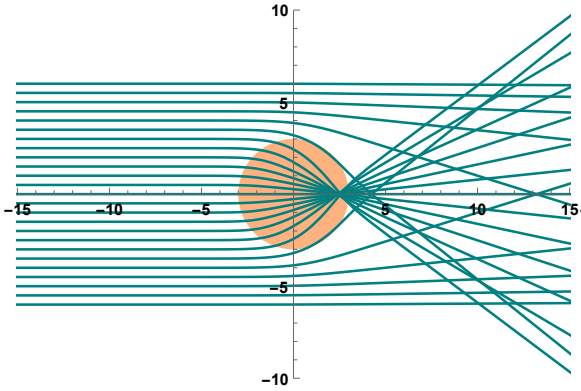


(a) Photon scattering for a warp drive with $\sigma = 1$

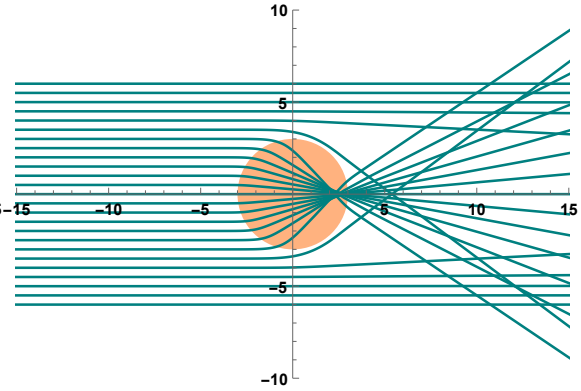


(b) Photon scattering for a warp drive with $\sigma = 2$

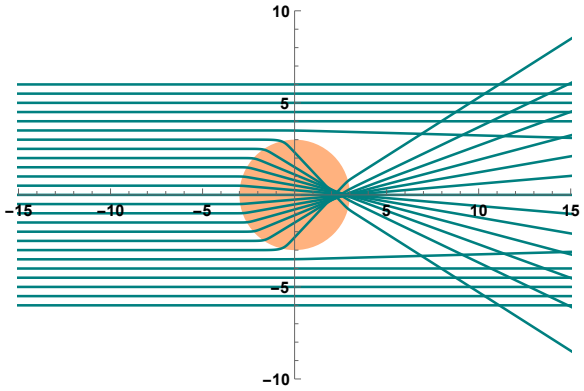


(c) Photon scattering for a warp drive with $\sigma = 5$

Figure 4.5: Ray trajectories for light in the $xy$-plane of the Alcubierre warp drive for warp speed $v = 1$ and variable warp bubble widths $\sigma \in \{1, 2, 5\}$. Light rays from infinity are shone parallel to the $x$-axis with light rays equally spaced with impact parameters ranging from -6 to 6. Parameter values: $v = 1$ and $R = 3$.

We observe two major differences in our ray tracing for different warp bubble width values. First, we observe that there is an evident change in the abruptness exhibited in the transition of the ray trajectories to the $x$-axis extending to its propagation back to infinity. In the light ray's interaction with the Alcubierre wrap drive with $\sigma = 1$ the transition to the $x$-axis axis and the opposite $y$-region exhibited a more defined curve as compared to the $\sigma = 2$, and $\sigma = 5$ cases. For higher values of $\sigma$, the steepness of the trajectories increases, resulting to a more abrupt transition. Recall our discussions about Alcubierre's choice for $f(r)$ and $\sigma$. Meanwhile, when we decrease the value of the warp bubble width, we expect the ray trajectories to

exhibit a more relaxed transition, as compared to the sudden transition for higher values of the bubble width.

Second, we observe that there is a significant difference in the angular deflections exhibited by light for different values of the warp bubble width for both the strong and weak lensing mechanisms in the warp drive distortion. The apparent change in the deflection angles is more noticeable for photons that exhibit a weak lensing effect in the warp drive. As the $\sigma$ value is increased there is a corresponding decrease in the angular deflection experienced by photons outside the warp bubble radius. We expect that for larger values of the warp bubble width the impact parameters just outside the warp bubble radius would experience less and less deflection until it reaches the deflection angle value of zero. This means that other than the steepness of our transition, our choice of $\sigma$ also affects the immediate region that the Alcubierre warp drive influences.

## 4.4 Deflection angles for variable warp bubble width

The angular deflections of photons of different impact parameters for a warp bubble with constant speed and different warp bubble widths is shown in Fig. (4.6). As we have discussed earlier, photons that have an impact parameter of $b = 0$ wouldn't experience any deflection but as we increase the magnitude of the impact parameters there is gradual increase in the resulting angular deflections. However, when the magnitude of the impact parameters reaches its critical value there is a sudden decrease in angular deflection that reaches zero as we continue to increase the value of the impact parameters. The gradual increase grows slower as we increase the value of the warp bubble width. At the same time, the steep decrease in angular deflections grows steeper as we increase the value of warp bubble width. The figure also shows that the vicinity of the warp bubble also becomes smaller since there is an abrupt decrease in the measured values deflection angles, reaching a zero angular deflection, as the $\sigma$ value is increased. We can then expect that for higher values of the bubble width there would be less distortions in the vicinity of the warp bubble as the angular deflections of photons would approach the value of zero. The critical value of the impact parameter also approaches the value of zero as the $\sigma$ value is increased.

We also observe that for a warp bubble with increasing values of the warp bubble

width, there is an overall decrease in the angular deflections except for a small region where the angular deflection peaks because of its critical impact parameter value. We observe that the peaks for different values of $\sigma$ only differs by a small amount.

The choice of the warp bubble radius $R$ in this chapter does not directly affect the trend of the photon's angular deflections. We expect that photon deflections would follow the same trend observed in Figs. (4.4) and (4.6) for warp drives of different warp speed and warp bubble thickness, but for an entirely different set of photon impact parameters.

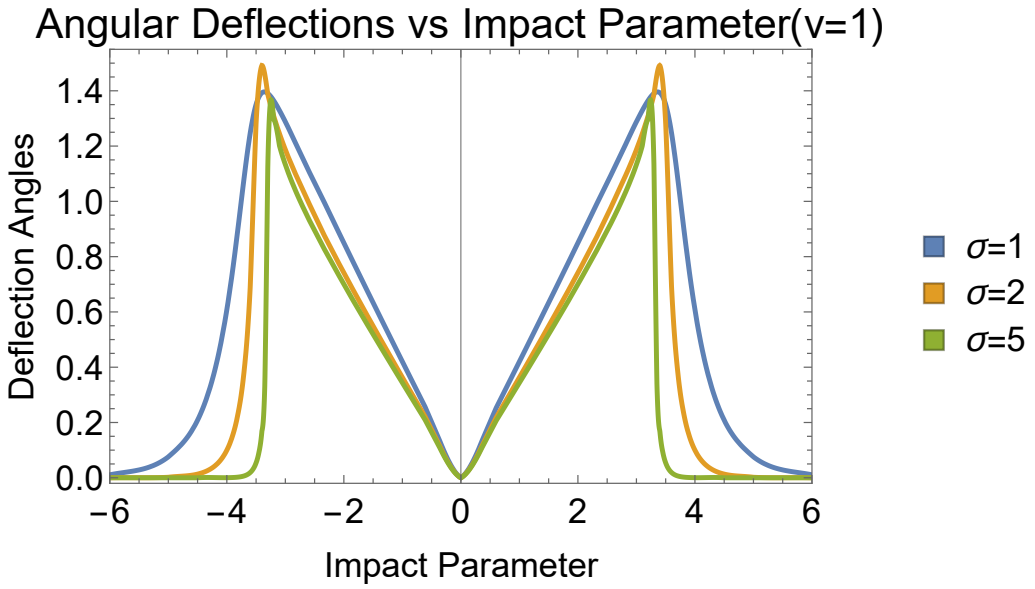


Figure 4.6: Deflection angles of photons of different impact parameters for a warp drive distortion with different warp bubble width values. Parameter values: $v = 1$ and $R = 3$.

# Chapter 5

# Energy shifts of photons in the Alcubierre warp drive

## 5.1 Energy shifts for variable warp speeds

In relativity, the energy-momentum four-vector is given by:

$$p_\mu = \left(\frac{E}{c}, p_x, p_y, p_z\right) \tag{5.1}$$

This means that we can consider the $p^t$ component of our photon four-momentum to study the shifts in energy for light that propagates through the Alcubierre war drive. Fig. [5.1a - 5.1d] shows how the energies of photons of different impact parameters shift before, during, and after its interaction with the Alcubierre warp drive for different values of v and a constant value of $\sigma = 1$. It is found that as light propagates through a warp drive it blue-shifts upon approach, then red-shifts upon exit. Additionally, the photon's interaction with the warp bubble leaves an overall net blue-shift that is both unexpected and interesting. Physically these energy shifts correspond to a change of color of physical light as the wave length and energy of light would change accordingly.

Photons exhibit a big increase in energy as it interacts with the warp drive then would experience a gradual decrease as the photon leaves the warp drive vicinity. Notice that the shifts in energy would start earlier as the the warp speed is increased. This is due to the earlier interaction between the photons and the warp drive as earlier discussed in Chapter IV. The photon energy values peak when the $b = 0$ photon is in the bridge of the warp bubble and verifies the results done in [49,50]. According to the following papers, the energy of the photons would peak with a

value of $v + 1$ at the center of the warp bubble for photons that would interact with an incoming Alcubierre warp distortion.

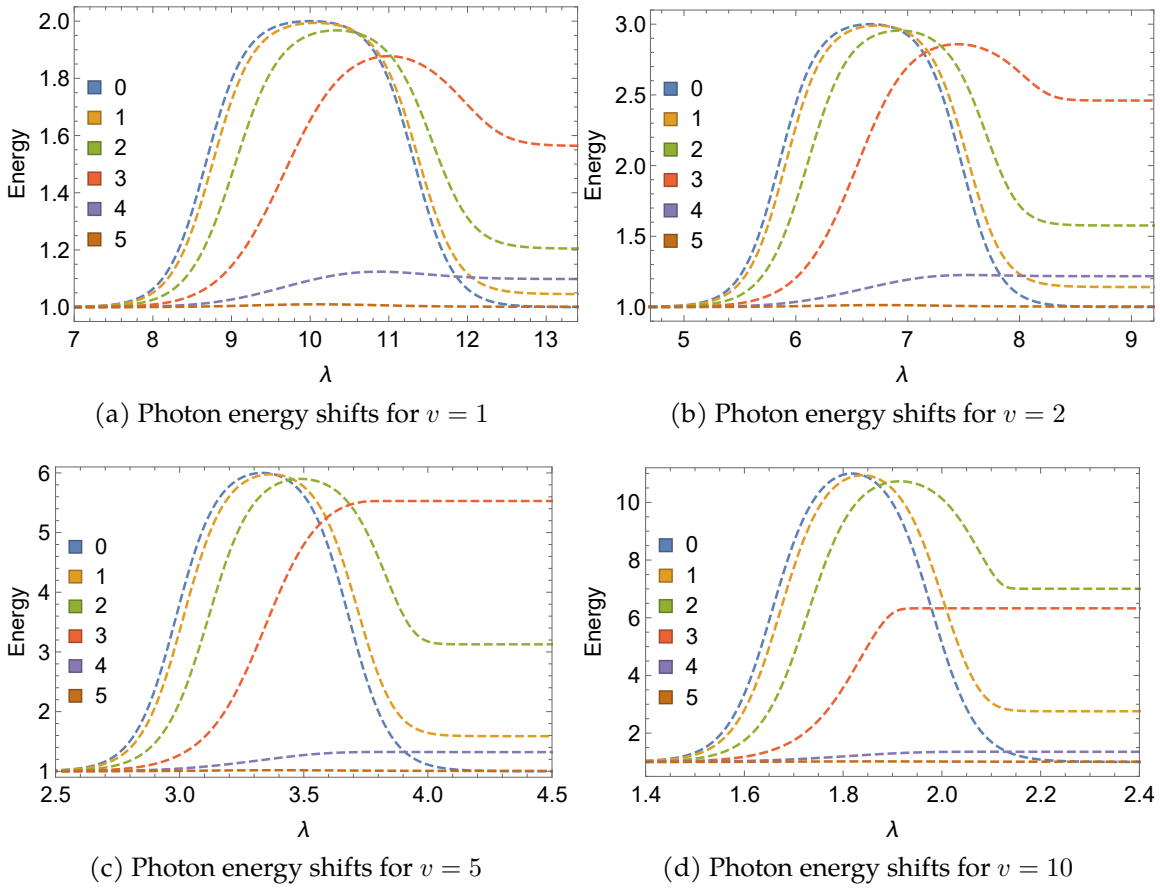


(a) Photon energy shifts for $v = 1$

(b) Photon energy shifts for $v = 2$

(c) Photon energy shifts for $v = 5$

(d) Photon energy shifts for $v = 10$

Figure 5.1: Energy vs arbitrary variable, $\lambda$, of photons of different impact parameters for warp speeds values $v \in \{1, 2, 5, 10\}$. Parameter values: $\sigma = 1$ and $R = 3$.

Our discussions in Chapter IV pertaining to the critical impact parameter values of photons interacting with the wrap drive still applies to the photon energy shifts. The photons with impact parameter magnitudes less the critical impact parameter value would experience a greater increase in energy. Meanwhile, photons with impact parameter magnitudes greater than the critical impact parameter value would experience less increase in energy. In the next section, we will further discuss the overall blue-shifts of photon energies as the warp speed is increased.

## 5.2 Overall blue-shift for variable warp speeds

The overall blue-shift of energies mentioned in the previous section is shown in Fig. (5.2). The overall blue-shift is measured for warp speed values $v \in \{1, 2, 510\}$

and a constant warp bubble width $\sigma = 1$ At first look, we see that the blue-shifted energies increase as the warp speed is increased. Similar to our discussion in the effects of the increase in warp speed to our deflection angle results, we see that there is a gradual increase in the overall blue-shift values, peaking with a $v + 1$ value at critical impact parameter values, then finally experiencing a steep decrease as the photon impact parameter leaves the vicinity of the warp drive. The changes in value of the final energies with respect to the photon's impact parameter becomes steeper as the warp speed is increased. The gradual increase slowly becomes steeper before reaching the peak, while the sharp decrease becomes more pronounced before reaching the value of zero. As observed earlier, the magnitude of the critical impact parameter decreases and approaches the asymptotic value of zero as the warp speed is increased.

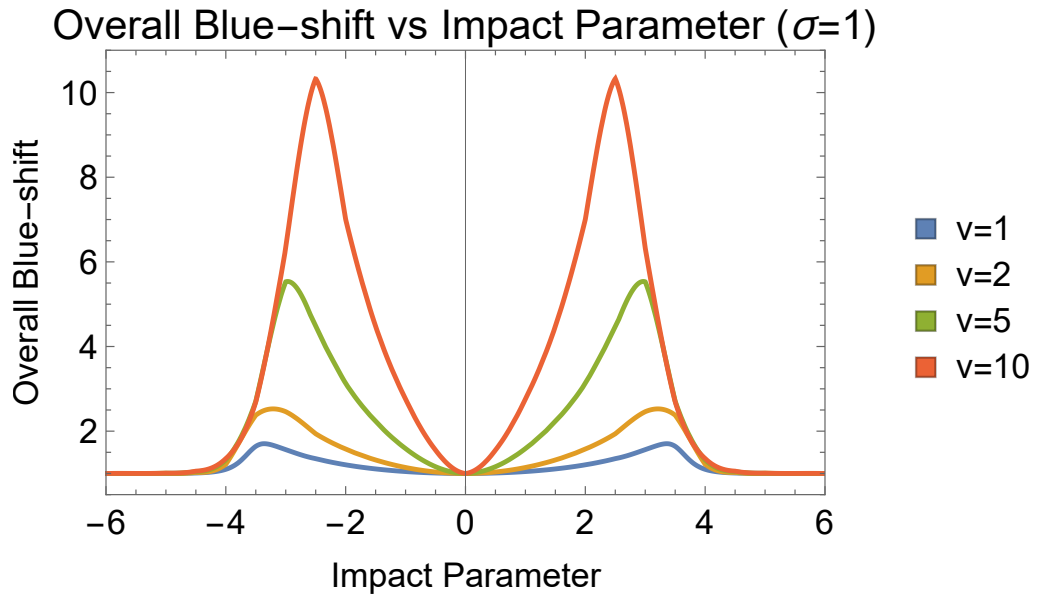


Figure 5.2: The final energies or overall blue-shifts in photon energies vs impact parameter for different warp speed values. Parameter values: $\sigma = 1$ and $R = 3$.

## 5.3 Energy shifts for variable warp bubble width

Figs. (5.3a - 5.3c) shows the shifts in energy with respect to an arbitrary variable, $\lambda$, as photons interact with Alcubierre warp drives with different warp bubble width values. The warp speed velocity is set at a constant value $v = 1$ for all three cases to properly highlight the effects of the warp bubble width on the photon energy shifts. We choose to study the energy shifts of photons with impact parameters

$b \in \{0, 1, 2, 3, 4, 5\}$.

The shifts in energy start to resemble our choice for $f(r)$ as our photons reach the vicinity of the of the warp bubble. It follows the trend shown by Fig. (2.1) in our discussions in Chapter II as the energy shifts begin to exhibit steeper energy transitions of photons from flat space to the vicinity of the warp bubble, and vice versa, as the warp bubble width is increased.

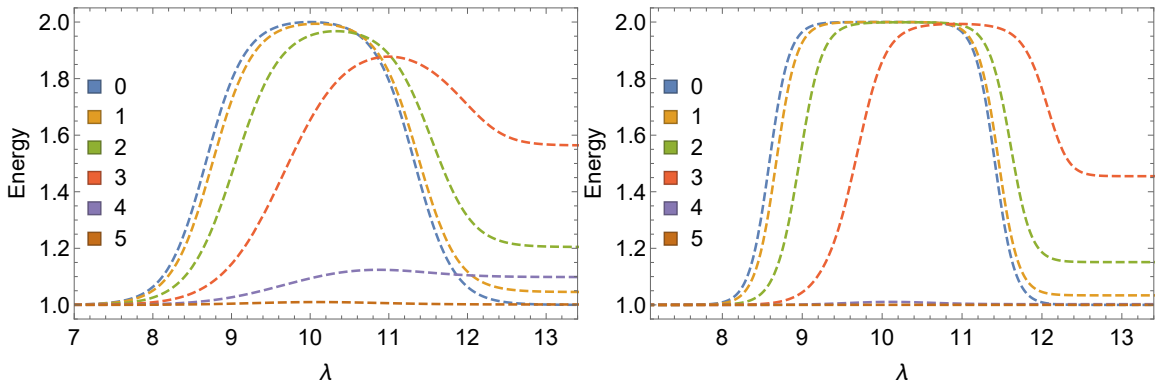


(a) Photon energy shifts for $\sigma = 1$

(b) Photon energy shifts for $\sigma = 2$

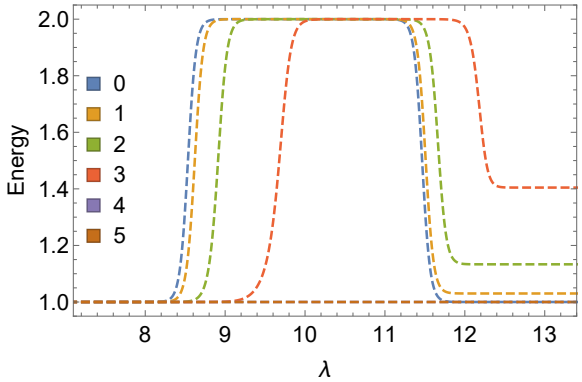


(c) Photon energy shifts for $\sigma = 5$

Figure 5.3: Energy vs arbitrary variable, $\lambda$, of photons of different impact parameters for warp bubble width values $\sigma \in \{1, 2, 5\}$. Parameter values: $v = 1$ and $R = 3$.

It is also observed that the energy shifts of photons interacting with the warp drive that experiences strong lensing would have a greater energy peak, eventually reaching the value $v + 1$, as the warp bubble width is increased. We also observe that for thicker warp bubble width, photon energies would quickly transition to a $v + 1$ peak energy and retain this energy until it leaves the warp bubble. Meanwhile, photons who experience weak lensing would experience lesser changes in energy. This implies that photons that experience strong lensing will have a close to constant

energy value inside the warp bubble before experiencing a red-shift as it leaves the warp bubble vicinity.

However, despite the increase in the peak value of the photon energy shifts, we observe that there is an apparent decrease in the overall blue-shift of energies for photons that experience strong lensing. This will be further discussed in the next section.

## 5.4 Overall blue-shift for variable warp bubble width

The overall blue-shift of energies for photons of different impact parameter interacting with an Alcubierre warp drive with different warp bubble width is given by Fig. (5.4). As similarly observed in our other results, the resulting final energies is highly dependent on the photon's impact parameter. We observe that photons with impact parameter $b = 0$ does not experience an overall blue-shift as we observe in the previous section's Figs. (5.3a - 5.3c) that it returns to its initial energy value due to red-shifting after reaching its peak. For photons with impact parameter whose magnitude are between zero and the critical impact parameter value, we observe a gradual increase in the final energy values before reaching its peak. The final energy values would then experience a steep decrease for photons that have an impact parameter greater than the critical value.

The figure below also affirms our initial observation from the previous section about the apparent decrease in the overall blue-shift of photon energies as the warp bubble width is increased.

Similar to what we observed in Section 5.4, we observe that the increase in warp bubble width would result to a general decrease in the overall blue-shift of photons in the warp bubble. However, similar to our results in Chapter V, there is a small exempted region wherein the overall blue-shifted energy values would peak due to the critical impact parameter value. We expect that the peak reaches a value close to the discussed $v+1$ value before experiencing the steep falloff in values. Additionally, the critical impact parameter values asymptotically approaches the origin value of $b = 0$ as the warp bubble width is increased.

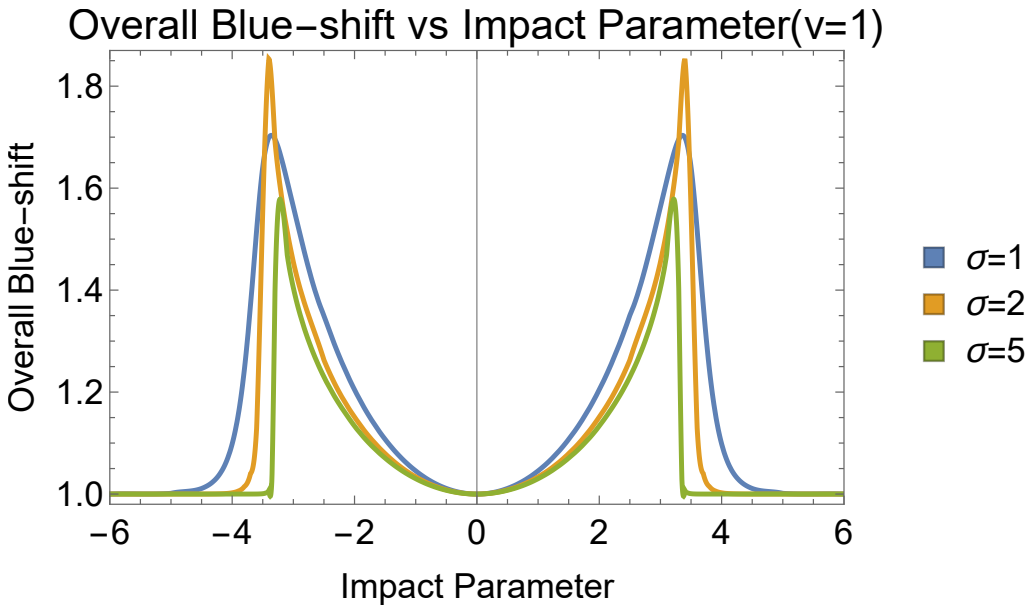


Figure 5.4: Overall blue-shifted energies for photons of different impact parameter interacting with an Alcubierre wrap drive of different warp bubble width values. Parameter values: $v = 1$ and $R = 3$.

# Chapter 6

# Conclusions and Recommendations

## 6.1 Summary and Conclusions

We performed numerical calculations to solve the equations of motion for photons that interact with an Alcubierre warp drive using Lagrangian-based geodesics in Chapter III. Using parametric plots, we were able to use these equations of motion to effectively visualize the scattering that happens to photons around the vicinity of a warp bubble distortion. We then tried to replicate the photon scattering results of Anderson et al. [23] for an Alcubierre warp drive with radius $R = 3$ and warp bubble thickness $\sigma = 5$. We have shown in Chapter III that the Lagrangian-based method that we used in our calculation gives the same level of accuracy when solving for the photon scattering in the warp drive when compared with the Hamiltonian-based method that Anderson primarily utilized for their work.

We showed in Chapter IV and V that the warp velocity and warp bubble thickness plays a huge role in the scattering of light in the warp drive distortion. In Chapter IV we studied the effects of changing values of the warp velocity and warp bubble thickness to the overall trajectory and angular deflection of photons interacting with the warp drive distortion. We find that photons experience an increase in angular deflections as the warp velocity is increased - reaching the asymptotic value of $\pi/2$ - and a corresponding overall decrease in angular deflection as the warp bubble thickness is increased. Additionally, we find that the peak of the angular deflections approach the asymptotic value of $b = 0$ when the warp velocity and warp bubble thickness values approach infinity.

In Chapter V, we studied the effects of changing the same parameters to the energy shifts and overall blue-shifts of photons in the warp drive distortion. We

find that photons experience a blue-shift that starts as it enters the vicinity of the warp bubble, and a corresponding red-shift as it leaves the region of distorted space. The $b = 0$ photon (the photon that passes through the bridge of the warp bubble) reaches a value of $v + 1$ before getting red-shifted and returning to its original energy. Meanwhile, the photon described by the critical impact parameter value of the system reaches the same $v + 1$ energy and maintains that value as the photon leaves the warp bubble. Additionally, we observe that photons inside the vicinity of the warp drive would reach the same $v + 1$ value, following the trend described by the shape function $f(r)$, once the warp bubble thickness is increased. We find that photons experience an general increase in its overall blue-shift when the warp velocity is increased, and a corresponding decrease when the warp bubble width is thickened.

## 6.2 Recommendations

We can extend this thesis further by providing a more effective light-ray-tracing map in *Mathematica* to construct images of the view of an observer near an Alcubierre warp drive to better visualize the image distortion that happens in this unique space-time curvature as similarly done in [51] for an image that passes through *Interstellar*'s wormhole. Next, we can consider firing charged particles, such as protons and electrons, that exhibits positive (+) and negative (-) charges, respectively. Since we only considered uncharged particles in this thesis, it is exciting to see if there is a significant difference in the scattering and deflection in the Alcubierre warp drive for charged particles. This would only require a small modification in the geodesic equation as we would only be require to add an electromagnetic field strength tensor term to solve for the equations of motion of our test particles. It is also interesting to study the motion of more massive objects through an Alcubierre warp drive. The question to be answered is, "Would more massive objects, such as stars, experience a similar deflection or would it start to orbit around the Alcubierre warp drive distortion?" Finally, we can consider an Alcubierre warp drive filled with dense matter, plasma for example, instead of vacuum inside the warp bubble. We can then study the difference in both the angular deflection and energy shifts for such change in our system. All of these questions in the hopes of gaining a better understanding of this special Alcubierre warp drive space-time curvature.

# Appendix

## Properties of the Alcubierre warp drive

The most interesting property of the Alcubierre warp drive is it allows faster-than-light travel. Although special relativity has a restriction that nothing can travel faster thank light, the unique curvature exhibited in the Alcubierre warp drive allows an object to reach apparent speeds faster than light from the point of view of an observer outside the vicinity of the warp drive. However, it never actually exceeds the speed restriction in its own local reference frame which is acceptable in general relativity. This can be shown by calculating the light cones of the Alcubierre warp drive metric. Consider a warp drive in two dimensions that moves in the positive $x$-direction. We have a metric that is given by

$$ds^2 = -dt^2 + [dx - vf(r)dt]^2 \tag{1}$$

The light cones correspond to the space-time intervals wherein $ds^2 = 0$.

$$dt^2 = [dx - vf(r)dt]^2 \tag{2}$$

$$\pm\, dt = dx - vf(r)dt \tag{3}$$

We can then solve for $dx/dt$.

$$\frac{dx}{dt} = \pm 1 + vf(r) \tag{4}$$

A space ship inside the Alcubierre warp drive would essentially ride the warp drive distortion moving in the same superluminal speed as the warp velocity. Therefore $v$ would also describe how fast the space ship is moving to an observer outside the warp drive distortion. We can then conclude that

$$v - 1 < v < v + 1 \tag{5}$$

This means that although it may appear that the space ship is travelling faster than light to an outside observer, the object locally is moving within its light cone. This

happens because the light cones are "tipped" due to the warp drive distortion. In a space time diagram, the light cones follow the slopes given in Eqn. (4).

Another interesting property in the warp drive is that the space ship in the warp drive will move as if it is in free fall. The space ship inside the warp bubble will feel no tidal forces because the warp bubble is a region of flat space. As an example, consider the center of the warp bubble, $r = 0$. In this region, $f(r) = 1$. Therefore the metric tensor becomes

$$g_{\mu\nu} = \begin{pmatrix} -1+v^2 & -v & 0 & 0 \\ -v & 1 & 0 & 0 \\ 0 & 0 & 1 & 0 \\ 0 & 0 & 0 & 1 \end{pmatrix} \tag{6}$$

Since we are using a constant value of the warp speed $v$, the Christoffel simply vanish. This means that the space ship is experiencing free fall.

A third interesting property is that the proper time of a spaceship inside the warp drive is equal to the coordinate time. This is unusual in special relativity because we would expect an object moving faster than light to experience time dilation. To show this, we can use the definition of the proper time:

$$\tau = \int_0^T -g_{\mu\nu} dx^\mu dx^\nu \tag{7}$$

$$= \int_0^T \left(dt^2 - [dx - vf(r)dt]^2\right)^{\frac{1}{2}} \tag{8}$$

For the spaceship riding at the center of the warp bubble, $f(r) = 0$. The warp velocity is also defined as $v = dx/dt$. The proper time reduces to

$$\tau = \int_0^T \left(dt^2 - [dx - \frac{dx}{dt}dt]^2\right)^{\frac{1}{2}} \tag{9}$$

$$= \int_0^T (dt^2)^{\frac{1}{2}} \tag{10}$$

$$= T \tag{11}$$

## Volume expansion of the Alcubierre warp drive

For hypersurfaces such as the Alcubierre warp drive, there is an aspect of the geometry that describes how it is embedded in the the $4$-dimensional space-time surrounding it. This aspect of the geometry is something that cannot be described

by intrinsic measurements on the hypersurface such as lengths, areas, and volumes, and is known as the *extrinsic geometry* of the hypersurface.

In order to fully describe the extrinsic aspect of the hypersurface geometry, we are tasked to define the extrinsic curvature tensor, $K_{ij}$, of the hypersurface. The extrinsic curvature of a hypersurface in a surrounding space-time measures how much projected gradients of the normal vectors differ at different points in the hypersurface. Therefore, it describes the rate at which the hypersurface deforms as it is extended along normal vectors.

The metric and the extrinsic curvature tensor are considered as the equivalent of the positions and velocities in classical mechanics because they measure the instantaneous state of the gravitational field. They are usually referred to as the first and second fundamental forms, respectively. The extrinsic curvature tensor is defined as:

$$K_{ij} = \frac{1}{2\alpha}\left(D_i\beta_j + D_j\beta_i - \frac{\partial g_{ij}}{\partial t}\right) \tag{12}$$

where $D_i$ denotes the covariant differentiation with respect to the 3-metric $\gamma_{ij}$. From the given values of $\alpha$ and $\gamma_{ij}$, the expression above simplifies into

$$K_{ij} = \frac{1}{2}\left(\partial_i\beta_j + \partial_j\beta_i\right) \tag{13}$$

According to Baumgarte [30], the negative of the trace of the extrinsic curvature, usually called as the mean curvature, measures the fractional change in the proper three-volume along the normal. We can then look for a function that represents the volume expansion of the warp drive distortion using the mean curvature.

$$\theta = -\alpha \operatorname{Tr} K \tag{14}$$

Where the trace of K corresponds to

$$\operatorname{Tr} K = K_{11} + K_{22} + K_{33} \tag{15}$$

From the given values of $\beta^x$, $\beta^y$ and $\beta^z$, we can simplify the above expression into

$$\theta = -\alpha\left(\partial_x\left(-v_s f(r_s) + 0 + 0\right)\right) \tag{16}$$

As mentioned in Chapter II, we set our value for the lapse function to be $\alpha = 1$. Plugging in this value while using the relation (17) for the evaluation of the partial derivative shown above, we arrive with the following result (18).

$$\frac{\partial f(r_s)}{\partial x} = \left(\frac{\partial f(r_s)}{\partial r_s}\right)\left(\frac{\partial r_s}{\partial x}\right) \tag{17}$$

$$\theta = v_s \left( \frac{\partial f(r_s)}{\partial r_s} \right) \left( \frac{\partial r_s}{\partial x} \right) \tag{18}$$

Further simplifying the above expressions leaves us with

$$\theta = v_s \left( \frac{x - x_s}{r_s} \right) \left( \frac{df}{dr_s} \right) \tag{19}$$

We can then plot this volume expansion to have a better visual of the Alcubierre warp drive distortion in a surrounding three-dimensional space.

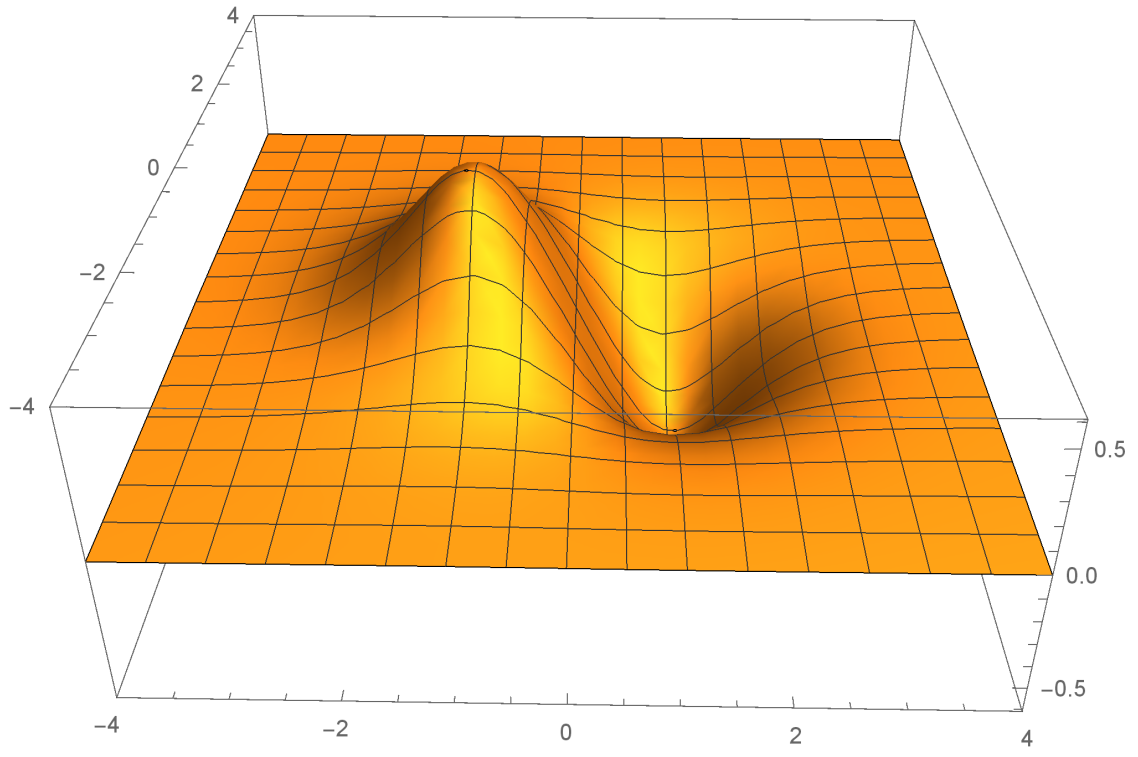


Figure 1: Volume expansion of the Alcubierre warp drive for $\sigma = 1$ and $R = 3$.

# Physical limitations in a warp drive

For this discussion we shall utilize a modified version of the piece-wise function, $f(r_s)$, given by Pfenning and Ford in their discussion on the energy restrictions

required to sustain an Alcubierre warp drive [18]

$$f_{mod}(r_s) = \begin{cases} 1 & r_s < R - \frac{\Delta}{2} \\ -\frac{1}{\Delta}(r_s - R - \frac{\Delta}{2} & R - \frac{\Delta}{2} < r_s < R + \frac{\Delta}{2} \\ 0 & r_s > R + \frac{\Delta}{2} \end{cases} \tag{20}$$

where again $R$ is the radius of the bubble. The variable $\Delta$ is defined as the bubble wall thickness and is related to the bubble width $\sigma$ and is defined as

$$\Delta = \frac{[1 + tanh^2(\sigma R)]^2}{2\sigma tanh(\sigma R)} \tag{21}$$

which in the limit of large values for $\sigma R$ will have an approximate value $\Delta = 2/\sigma$.

In this modified Alcubierre shape form, we see that inside the warp bubble, where $r_s < R - \frac{\Delta}{2}$, every observer would ride the warp wave and travel at the same speed as the warp bubble. So any spaceship that reaches the interior of the warp bubble would ride the distortion essentially moving at apparent faster-than-light speeds. Meanwhile, for observers whose trajectories that pass only through the walls of the bubble, $R - \frac{\Delta}{2} < \rho < R + \frac{\Delta}{2}$, the result is identical to the trajectories found in the Alcubierre shape function. This region contains the bulk of the negative energy required to sustain the existence of warp drive.

We then consider the negative energy density distribution of the Alcubierre warp drive metric. Miguel Alcubierre in his paper [11] presented the needed negative energy density needed to sustain the said space-time distortion

$$\langle T^{\mu\nu} u_\mu u_\nu \rangle = \langle T^{00} \rangle = \frac{1}{8\pi} G^{00} = -\frac{1}{8\pi} \frac{v_s^2(t)\rho^2}{4r_s^2(t)} \left( \frac{df(r_s)}{dr_s} \right)^2 \tag{22}$$

where $\rho = \sqrt{y^2 + z^2}$, is the radial distance perpendicular in the $yz$-plane, perpendicular to the $x$-axis. We then show that the energy density that would be measured by an observer in a spaceship is always negative as seen from the above expression.

We shall then look at the total amount of negative energy that is needed to sustain the Alcubierre warp drive metric. Let us consider a warp bubble that moves in the $x$-direction with constant velocity $v_b$ such that $x_s(t) = v_s t$. Since we set the total energy to be constant, we can calculate the total energy at any time and not worry about discrepancies in the calculation. For this study we calculate the total energy at time $t = 0$ for simplification. With this, we then have

$$r_s(t = 0) = [x^2 + y^2 + z^2]^{\frac{1}{2}} = r \tag{23}$$

The integral of the local matter energy density over the proper volume can then be written as

$$E = \int dx^3 \sqrt{g} \langle T^{00} \rangle = -\frac{v_b^2}{32\pi} \int \frac{\rho^2}{r^2} \left( \frac{df(r)}{dr} \right)^2 dx^3 \tag{24}$$

where $g = \det g_{ij}$ is the determinant of the spatial metric on the constant time hypersurfaces. We can simplify this integral by transforming our cartesian coordinates to spherical coordinates. Doing so reduces the integral into

$$E = -\frac{1}{12} v_b^2 \int_0^\infty r^2 \left( \frac{df(r)}{dr} \right)^2 dr \tag{25}$$

We can then use the piece-wise continuous approximation of the shape function given by (20) since we are only estimating the order of magnitude of the total energy. When we take the derivative of the shape function, we find out that the negative energy contribution only comes from the wall of the warp bubble. We then come up with the evaluation

$$E = -\frac{1}{12} v_b^2 \int_{R-\frac{\Delta}{2}}^{R+\frac{\Delta}{2}} r^2 \left( \frac{-1}{\Delta} \right)^2 dr \tag{26}$$

$$= -\frac{1}{12} v_b^2 \left( \frac{R^2}{\Delta} + \frac{\Delta}{12} \right) \tag{27}$$

Pfenning and Ford also considered the total energy needed to sustain a warp drive. The warp drive they discussed was 100 meters long so that it may fit a hypothetical spaceship inside. It has been shown in their study that the wall thickness is constrained by

$$\Delta \leq 100 v_b^2 L_{planck} \tag{28}$$

where $L_{planck}$ is the Planck length.

If we decide to use the given constraint and set our warp bubble to be 100 meters, we can then neglect the second term in (27) as the second term is significantly small unless we set our warp speeds to be approximately of magnitude $10^9$ meters and above. Then it follows that

$$E \leq -6.2 \times 10^{70} v_b L_{Planck} \sim -6.2 \times 10^{65} v_b \text{grams} \tag{29}$$

Since a typical galaxy has an approximate mass of

$$M_{MilkyWay} \approx 10^{12} M_{Sun} = 2 \times 10^{45} \text{grams} \tag{30}$$

the energy required for the maintenance of a warp bubble is in the order of

$$E \leq -3 \times 10^{20} M_{MilkyWay} v_b \tag{31}$$

We then see that the total amount of negative mass needed to sustain an Alcubierre warp drive is magnitudes greater than the mass of the entire visible universe.

We further conclude that a more practical warp drive can be considered but the minimum total energy needed by a warp drive is still a quarter of a solar mass to be attainable which is still far beyond our reach.

# Bibliography


[1] José Natário. Warp drive with zero expansion. *Classical and Quantum Gravity*, 2002.

[2] Michael S. Morris and Kip S. Thorne. Wormholes in spacetime and their use for interstellar travel: A tool for teaching general relativity. *American Journal of Physics*, 1988.

[3] Matt Visser. Traversable wormholes: Some simple examples. *Physical Review D*, 1989.

[4] Matt Visser. Traversable wormholes from surgically modified Schwarzschild spacetimes. *Nuclear Physics, Section B*, 1989.

[5] Matt Visser. *Lorentzian wormholes: From Einstein to Hawking*. 1995.

[6] S. V. Krasnikov. Hyperfast travel in general relativity. *Physical Review D - Particles, Fields, Gravitation and Cosmology*, 1998.

[7] Allen E. Everett and Thomas A. Roman. Superluminal subway: The Krasnikov tube. *Physical Review D - Particles, Fields, Gravitation and Cosmology*, 1997.

[8] José P.S. Lemos, Francisco S.N. Lobo, and Sérgio Quinet De Oliveira. Morris-Thorne wormholes with a cosmological constant. *Physical Review D*, 2003.

[9] José P.S. Lemos and Francisco S.N. Lobo. Plane symmetric traversable wormholes in an anti–de Sitter background. *Physical Review D - Particles, Fields, Gravitation and Cosmology*, 2004.

[10] Francisco Lobo and Paulo Crawford. Weak Energy Condition Violation and Superluminal Travel. 2003.

[11] Miguel Alcubierre. The warp drive: hyper-fast travel within general relativity. 2000.

[12] Ken D. Olum. Superluminal travel requires negative energies. *Physical Review Letters*, 1998.

[13] Matt Visser, Bruce Bassett, and Stefano Liberati. Perturbative superluminal censorship and the null energy condition. 2009.

[14] Matt Visser, B. A. Bassett, and S. Liberati. Superluminal censorship. *Nuclear Physics B - Proceedings Supplements*, 2000.

[15] Carlos Barceló and Matt Visser. Twilight for the energy conditions? *International Journal of Modern Physics D*, 2002.

[16] Carlos Barceló and Matt Visser. Scalar fields, energy conditions and traversable wormholes, 2000.

[17] Carlos Barceló and Matt Visser. Traversable wormholes from massless conformally coupled scalar fields. *Physics Letters, Section B: Nuclear, Elementary Particle and High-Energy Physics*, 1999.

[18] M. J. Pfenning and L. H. Ford. The unphysical nature of 'warp drive'. *Classical and Quantum Gravity*, 14(7):1743–1751, 1997.

[19] L. H. Ford and Thomas A. Roman. Averaged energy conditions and quantum inequalities. *Physical Review D*, 1995.

[20] L. H. Ford and Thomas A. Roman. Quantum field theory constrains traversable wormhole geometries. *Physical Review D - Particles, Fields, Gravitation and Cosmology*, 1996.

[21] Chris Van Den Broeck. On the (im)possibility of warp bubbles. (im), 1999.

[22] Francisco S.N. Lobo and Matt Visser. Fundamental limitations on 'warp drive' spacetimes. *Classical and Quantum Gravity*, 21(24):5871–5892, 2004.

[23] Tom H. Anderson, Tom G. MacKay, and Akhlesh Lakhtakia. Ray trajectories for Alcubierre spacetime. *Journal of Optics*, 13(5):1–15, 2011.

[24] Edmund Bertschinger. Introduction to Tensor Calculus for General Relativity. pages 1–34, 2000.

[25] Robert M. Wald. *General Relativity*. The University od Chicago Press, 1984.

[26] Bernard Schutz. *A First Course in General Relativity*. 2009.

[27] James B. Hartle and Jennie Traschen. Gravity: An introduction to Einstein's general relativity. *Physics Today*, 2005.

[28] J.A. Wheeler C.W. Misner, Kip S. Thorne. Gravitation (Physics Series) - Charles W. Misner, Kip S. Thorne, John Archibald Wheeler -W. H. Freeman (1973).pdf.

[29] E Poisson. Spacetime and Geometry: An Introduction to General Relativity. *Classical and Quantum Gravity*, 2005.

[30] Thomas W. Baumgarte and Stuart L. Shapiro. *Numerical relativity: Solving Einstein's equations on the computer*. 2010.

[31] Sean Carroll. *Spacetime and Geometry: Pearson New International Edition: An Introduction to General Relativity*. 2014.

[32] Jerzy Plebanski. Electromagnetic waves in gravitational fields. *Physical Review*, 1960.

[33] M.O. Scully and W. Schleich. GENERAL RELATIVITY AND MODERN OPTICS. In *Les Houches Summer School on Theoretical Physics: New Trends in Atomic Physics*, pages 995–1124, 1982.

[34] Igor I. Smolyaninov. Metamaterial 'multiverse'. *Journal of Optics*, 2011.

[35] I. I. Smolyaninov and E. E. Narimanov. Optical models of the big bang and non-trivial space-time metrics based on metamaterials. In *Optics InfoBase Conference Papers*, 2010.

[36] Qiang Cheng, Tie Jun Cui, Wei Xiang Jiang, and Ben Geng Cai. An electromagnetic black hole made of metamaterials. pages 1–14, 2009.

[37] Miao Li, Rong Xin Miao, and Yi Pang. Casimir energy, holographic dark energy and electromagnetic metamaterial mimicking de Sitter. *Physics Letters, Section B: Nuclear, Elementary Particle and High-Energy Physics*, 2010.

[38] Tom G. MacKay and Akhlesh Lakhtakia. Negative refraction, negative phase velocity, and counterposition in bianisotropic materials and metamaterials. *Physical Review B - Condensed Matter and Materials Physics*, 2009.

[39] T. G. Mackay, A. Lakhtakia, and S. Setiawan. Electromagnetic waves with negative phase velocity in Schwarzschild-de Sitter spacetime. *Europhysics Letters*, 2005.

[40] T. G. Mackay, S. Setiawan, and A. Lakhtakia. Negative phase velocity of electromagnetic waves and the cosmological constant. *European Physical Journal C*, 2005.

[41] Igor I Smolyaninov. Surface plasmon toy model of a rotating black hole. *New Journal of Physics*, 2003.

[42] Tom G. Mackay, Akhlesh Lakhtakia, and Sandi Setiawan. Electromagnetic negative-phase-velocity propagation in the ergosphere of a rotating black hole, 2005.

[43] Serguei S. Komlssarov. Blandford-znajek mechanism versus penrose process, 2009.

[44] M. Sharif and Umber Sheikh. Cold plasma gravitomagnetic waves in a Kerr planar analogue. *Journal of the Korean Physical Society*, 2009.

[45] Benjamin M. Ross, Tom G. Mackay, and Akhlesh Lakhtakia. On negative-phase-velocity propagation in the ergosphere of a charged rotating black hole. *Optik*, 2010.

[46] M. Hossain Ali and M. Khayrul Hasan. Dispersion relations for cold plasmas around Reissner-nordström black holes. *International Journal of Theoretical Physics*, 2009.

[47] Tom G. Mackay and Akhlesh Lakhtakia. Towards a metamaterial simulation of a spinning cosmic string. *Physics Letters, Section A: General, Atomic and Solid State Physics*, 2010.

[48] Allan Greenleaf, Yaroslav Kurylev, Matti Lassas, and Gunther Uhlmann. Cloaking devices, electromagnetic wormholes, and transformation optics, 2009.

[49] Chad Clark, William A Hiscock, and Shane L Larson. Null geodesics in the Alcubierre warp drive spacetime: the view from the bridge. 1999.

[50] Michael Peter Kinach. Light Propagation in a Warp Drive Spacetime. Technical report, 2017.

[51] Oliver James, Eugénie von Tunzelmann, Paul Franklin, and Kip S. Thorne. Visualizing Interstellar 's Wormhole. *American Journal of Physics*, 83(6):486–499, jun 2015.